Applied Energy 402 (2026) 127056



Contents lists available at ScienceDirect

Applied Energy

journal homepage: www.elsevier.com/locate/apenergy

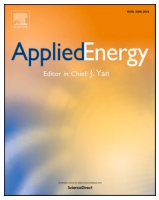



A few-shot learning framework for HVAC fault diagnosis in data centers with minimal data required

Ke Yan [a], Changfu He [a], Chuan Wang [a], Yuan Gao [b,*], Yang Du [c], Afshin Afshari [d]

[a] College of Mechanical and Vehicle Engineering, Hunan University, Changsha, China
[b] The Center for Energy Systems Design (CESD), International Institute for Carbon-Neutral Energy Research (WPI-I2CNER); Kyushu University, Japan
[c] College of Science and Engineering, James Cook University, Cairns, Australia
[d] Fraunhofer Institute for Building Physics, Fraunhoferstraße 10, 83626 Valley, Munich, Germany

HIGHLIGHTS

- A few-shot learning model is designed for HVAC systems in data centers with minimal required data.
- Semi-supervised learning approach is leveraged for class prototype updates without manual annotation.
- The proposed method delivers reliable automated HVAC fault diagnosis in data centers.

ARTICLE INFO

Keywords:
HVAC systems
Fault diagnosis
Few-shot learning
HVAC systems in data center
Prototype network

ABSTRACT

Fault diagnosis in heating, ventilation, and air conditioning (HVAC) systems is crucial for maintaining energy efficiency and reducing carbon emissions in data centers. Most existing data-driven HVAC fault diagnosis approaches depend on a sufficient quantity of labeled or unlabeled operational data. However, newly constructed data centers often lack both labeled and unlabeled HVAC operational data. Moreover, a review of the literature reveals that few-shot learning has received limited attention in the context of HVAC fault diagnosis for data centers with an extremely limited quantity of operational data. In this study, a semi-supervised adaptive weighted prototype network (SSAWPN) incorporating an attentive feature fusion approach is proposed for HVAC fault diagnosis in data centers with minimal data. First, a multi-scale attentive feature fusion network (MSAFN) leverages channel-wise segmentation, residual connections, and an attention mechanism to capture fault signatures across multiple spatial and temporal scales. Then, a semi-supervised adaptive weighted prototype optimization strategy (SAWPS) is employed to incrementally update class prototypes by assigning adaptive weights to unlabeled data. As new data accumulate, the prototypes become increasingly representative of actual fault modes without manual annotation. Lastly, real-world operational data from the chiller and air handling unit (AHU) are used to conduct ablation and comparative experiments. The experimental results show a clear advantage for SSAWPN in HVAC few-shot settings. It achieves mean F1 scores of 73.77 % on the ASHRAE RP1043 chiller fault severity level 1 dataset and 67.22 % on the ASHRAE RP1312 AHU summer dataset, outperforming the second-best approach by 3.21 and 1.35 percentage points, respectively.

1. Introduction

1.1. Background

In response to the growing computational demands of the digital era, the global deployment of data centers has accelerated considerably [1]. Recent statistics indicate that data centers contribute approximately 1 to 1.5 % of worldwide electricity consumption [2]. In light of the rapid expansion of artificial intelligence technologies, emissions associated with data centers are projected to rise to 3.2 % of global greenhouse gas emissions by 2025 [3]. According to the 2021 Energy Use Intensity (EUI) data by building type published in France, data centers exhibited an EUI of 2477 kWh/m^2, which is significantly higher than that of other building categories [4]. By 2030, the social cost associated with carbon emissions from data centers could amount to an estimated 125 to 140

* Corresponding author.
E-mail address: gao.yuan.564@m.kyushu-u.ac.jp (Y. Gao).

https://doi.org/10.1016/j.apenergy.2025.127056
Received 30 July 2025; Received in revised form 17 October 2025; Accepted 6 November 2025
Available online 14 November 2025
0306-2619/© 2025 The Authors. Published by Elsevier Ltd. This is an open access article under the CC BY license (http://creativecommons.org/licenses/by/4.0/).

Nomenclature

Abbreviations

AHU	Air handling unit
AI	Artificial intelligence
BN	Batch normalization
CF	Condenser fouling
CNN	Convolutional neural network
EO	Excess oil
EUI	Energy Use Intensity
FC	Fully connected
FWC	Reduced condenser water flow
FWE	Reduced evaporator water flow
GAN	Generative adversarial network
GAP	Global average pooling
HVAC	Heating, ventilation, and air conditioning
ML	Machine learning
MSAFN	Multi-scale attentive features fusion network
NC	Non-condensable in refrigerant
NM	Normal
PN	Prototype Network
RL	Refrigerant leakage
RO	Refrigerant overcharge
SAWPS	Semi-supervised adaptive weighted Prototype optimization strategy
SEM	Squeeze-excitation attention module
SL	Severity level
SMOTE	Synthetic minority oversampling technique
SSAWPN	Semi-supervised adaptive weighted prototype network
SSL	Semi-supervised learning
TL	Transfer learning

Symbols

$D_E[\cdot]$ & $D_E(\cdot)$	The square of the Euclidean distance
D_{TE}	Test set
D_{TR}	Training set
FN	The number of false negative samples
FP	The number of false positive samples
$F_{\mathrm{BN}}(\cdot)$	The batch normalization
$f_{\mathrm{Ca}}(\cdot)$	The feature combination operation
$f_{\mathrm{Conv}}(\cdot)$	The convolution operation
$f_{\mathrm{FC}}(\cdot)$	FC layer
$f_{\mathrm{Flatten}}(\cdot)$	The feature flattening operation
$f_{\mathrm{GAP}}(\cdot)$	The GAP layer operation
$f_{\mathrm{MaxPool}}(\cdot)$	Max pooling layer
$f_{\mathrm{Mish}}(\cdot)$	Mish activation function
$f_{\mathrm{ReLU}}(\cdot)$	ReLU activation function
$f_{\mathrm{SEM}}(\cdot)$	The SEM operation
$f_{\mathrm{Simoid}}(\cdot)$	Sigmoid activation function
$g_{a,i}$	The weight matrix when the feature vector of the i-th sample in the U is classified into class a
$h(\cdot)$	The feature vector of the data
$h_L(x)$	The feature vectors of the labeled data
$h_U(x)$	The feature vectors of the unlabeled data
L	The labeled dataset
n_a	The sample number of category a in the S
n_L	The number of samples in the L
n_Q	The number of samples of each category in the Q
n_S	The number of samples of each category in the S
n_U	The number of samples in the U
N_{TR}	The number of labeled samples drawn from each category
N_U	The number of unlabeled samples
P_a	The prototype of category a
Q	Query set
S	Support set
TN	The number of true negative samples
TP	The number of true positive samples
U	The unlabeled dataset
x	Input data
x_a	The data of category a
$x_{k,i}$	The i-th sample of the k-th category in the S
$x_{k,j}$	the j-th sample of the k-th category in the Q
$x_{\max}$	The maximum value of the x
$x_{\min}$	The minimum value of the x
x_{ne}	The normalized data
$y_{k,i}$	The corresponding label of the $x_{k,i}$
$y_{k,j}$	The corresponding label of the $x_{k,j}$
δ	The scaling factor
$*$	The element multiplication operation

billion annually [5].

Hyperscale data centers primarily support large-scale computing and internet services and are characterized by high-density server deployments and multi-tier redundancy. To ensure that core information and communication technology equipment operates within its specified environmental envelope, data centers rely on HVAC systems for the stable indoor conditions, including temperature, humidity and airflow levels. According to the literature survey, HVAC energy consumption typically accounts for 15 %–30 % of a data center's total energy use [6]. The American Society of Heating, Refrigerating and Air-Conditioning Engineers Thermal Guidelines [7] and materials from Lawrence Berkeley National Laboratory [8] specify recommended and allowable ranges for temperature and humidity in information technology equipment spaces. The recommended server inlet temperature is 18–27 °C, with an allowable range of 5–45 °C. The recommended relative humidity is 8–70 %, with an allowable range of 8–80 %. In industry practice, total supply airflow in data centers is typically on the order of 5000–10,000 m^3/min, with the exact value determined by installed capacity and thermal load. In real-world practices, several hyperscale data centers' operational constraints might contribute to high energy costs. These constraints include: (1) tight temperature and humidity bands to protect information technology equipment, (2) redundancy design that leads to frequent part-load operation of chillers and AHUs, and (3) improper hot/cold-aisle management, which reduces heating and cooling efficiency. These operational constraints require maintenance personnel for regularly monitoring of the performance and the condition of HVAC systems, resulting in a scarcity of available fault data.

Cooling systems within HVAC infrastructure represent one of the primary sources of energy consumption in data centers, accounting for nearly 40 % of total energy use [9]. At present, the intelligent management of data center cooling systems has emerged as a critical focus in energy management research [10]. Given that data centers need to operate 24/7, optimizing the operating status of the HVAC system is crucial to maintaining continuous and reliable operation of the data center [9,11]. As core components of the cooling system, AHUs regulate supply and return airflow and moisture, while chillers remove heat and maintain chilled-water setpoints. Their configuration, staging, and control are crucial for maintaining hyperscale data centers' temperature, humidity and airflow, thereby directly influencing operational reliability and energy efficiency of the data center.

Recently, artificial intelligence (AI) driven frameworks have made marked progress in optimizing HVAC system performance and fault diagnosis. These frameworks improve system efficiency, reduce energy consumption, and mitigate environmental impact through predictive

modeling, optimization, and fault diagnosis [12–15]. In the fields of predictive modeling and optimization, AI technology has yielded substantial research outcomes. For example, Lei et al. [16] studied temperature and humidity variation trends in HVAC systems across multiple building spaces and developed a predictive model for the operational status of a variable air volume HVAC system. Jung et al. [17] constructed a performance prediction model for the AHU system based on deep neural networks. Tang et al. [18] used deep learning models to automatically learn the operational characteristics of HVAC systems and combined thermodynamic knowledge to constrain the system's operating state. Zhang et al. [19] designed an interpretable machine learning method to increase the interpretability of the prediction process. Nisa et al. [20] analyzed variations in flow and temperature within HVAC systems, utilizing deep neural networks to predict the supply air temperature of the AHU system and the energy consumption of the chiller. Sulaiman et al. [21] applied the Kolmogorov-Arnold network to predict energy changes in chillers, yielding excellent predictive results. Lu et al. [22] developed an optimization control strategy based on reinforcement learning to optimize HVAC system operations in data centers. Guo et al. [23] developed a deep reinforcement learning optimization model to achieve HVAC system control optimization. Díaz et al. [24] incorporated system variables into the development of AI programs, enhancing the reliability of HVAC system operations. Ni et al. [25] used graph neural networks to analyze the relationships between HVAC system variables, ensuring indoor air quality in manufacturing facilities. Yao et al. [26] optimized variables such as airflow and temperature in HVAC systems to maintain indoor comfort. Ni et al. [27] explored the factors in HVAC systems that may affect system optimization performance. Ding et al. [28] employed neural networks to learn the dynamic characteristics of buildings, reducing energy losses. To enhance performance degradation prediction accuracy in data-scarce scenarios, Li et al. [29] developed a hybrid model based on a generative adversarial network (GAN) and the Informer algorithm.

As a key measure for improving HVAC efficiency and managing energy use, fault detection and diagnosis (FDD) have been extensively investigated in recent years. Despite significant progress in this area, several major challenges remain in practical applications. For example, for newly constructed data centers, data-driven FDD methods face significant challenges in collecting sufficient fault data due to their relatively short operational periods. Moreover, high-quality labeling of different categories of data requires operators to have extensive domain knowledge, and labeling fault data is a time-consuming and labor-intensive task. As a result, both labeled and unlabeled fault data are scarce in practical fault diagnosis scenarios in hyperscale data centers.

Table 1
Summary of existing works on HVAC system fault diagnosis.

Approaches	Characteristics	Limitations	References
Traditional rule-based	Good interpretability	Highly dependent on domain knowledge and operator expertise	[31–33]
Classical ML	Low computational complexity	Sensitive to feature engineering, domain shift, and sample size	[34–37]
Deep learning	Automatic feature extraction without manual design	Requires substantial training data for robust performance	[41,42]
Transfer learning	Suitable for fault diagnosis under varying operating conditions	Risk of negative transfer and requires careful model alignment	[38,39]
Generative-based	Increases the quantity and diversity of fault samples, helping to balance the dataset	Model training is challenging, performance is unstable, and the quality of generated data requires rigorous verification	[50–54]
Semi-supervised	Uses unlabeled data to further enhance model performance	Achieving good performance requires abundant unlabeled data	[55–63]

1.2. Literature review for fault diagnosis of HVAC systems

The fault diagnosis methods of chillers are generally categorized into rule-based methods and data-driven methods [30]. Deshmukh et al. [31] integrated expert rule-based fault detection techniques with thermodynamic principles to identify AHU faults. Tran et al. [32] designed a rule-based chiller fault identification method with good fault detection robustness. Lin et al. [33] employed active rules to improve the reliability of HVAC system fault diagnosis and combined them with multimodal data analysis techniques to further improve fault detection efficiency. Although rule-based fault diagnosis methods offer strong interpretability, they are highly dependent on prior knowledge and the technical expertise of the operators.

Driven by the rapid progress in smart sensing and advanced artificial intelligence technologies, data-driven methods have demonstrated increasingly promising solutions and clear advantages in HVAC fault diagnosis. Techniques for fault diagnosis based on machine learning (ML) are widely practiced in HVAC fault diagnosis. Han et al. [34] integrated support vector machines, random forests, and other methods to identify faults in chillers. Xia et al. [35] proposed a kernel entropy component analysis method to extract features and reduce the dimensionality of chiller fault data, leading to improved fault diagnosis results. Li et al. [36] utilized the extreme learning machine as the feature learner and combined it with the multi-label learning strategy to classify the faults of chillers. Simmini et al. [37] employed kernel principal component analysis and Gaussian kernel techniques to address the nonlinear characteristics of chiller data, enhancing the accuracy and generalization performance of the diagnostic method. With continual advances in deep learning, researchers are increasingly leveraging deep networks for HVAC fault diagnosis. Li et al. [38] applied transfer learning (TL) to chiller fault diagnosis by integrating it with domain-adaptive neural networks to enable fault diagnosis across different chiller systems. Liu et al. [39] carried out fault diagnosis under various TL tasks and verified the value of TL in chiller fault diagnosis. Zhu et al. [40] adopted the domain adaptive learning strategy to reduce the distribution differences of fault characteristics of different chillers. Jiang et al. [41] enhanced the diversity of fault samples to reduce the dependence of the diagnosis network on the source domain data and used the Transformer to extract the fault features of the chiller, achieving good diagnostic results. Miyata et al. [42] integrated the convolutional neural network (CNN) and the TL method to improve the diagnostic accuracy under different working conditions.

Although data-driven methods have achieved high diagnostic accuracy in HVAC fault diagnosis, their performance heavily relies on the availability of extensive labeled data [43–45]. Under conditions with limited labeled training data, the HVAC fault diagnostic results are significantly degraded [46,47]. Generative adversarial networks and semi-supervised learning (SSL) are two well-established approaches for addressing the challenge of limited labeled training data [48,49]. Du et al. [50] employed GANs to generate synthetic HVAC fault sample data, providing richer fault features for the diagnostic methods. Yan et al. [51] applied a conditional Wasserstein GAN to increase the chiller fault data and combined it with supervised learning technology to improve diagnostic accuracy. Zhang et al. [52] improved the quality of fault sample generation by using the variational autoencoder and GAN. Yan et al. [53] utilized a conditional Wasserstein GAN to generate the AHU data for the Transformer. Li et al. [54] developed an improved GAN to synthesize fault data and combined it with the semi-supervised diagnostic framework to lessen the dependence of the diagnostic model on labeled fault samples.

Semi-supervised learning (SSL) offers an effective solution to the

data scarcity challenge in HVAC fault diagnosis. Beghi et al. [55] employed a semi-supervised end-to-end network to detect and isolate chiller faults. Yan et al. [56] developed a semi-supervised fault diagnosis method to identify early-stage abnormalities in AHU, achieving promising results. Li et al. [57] designed a semi-supervised GAN to address the scarcity of labeled fault data in chiller fault diagnosis. Fan et al. [58] presented a self-training-based semi-supervised approach that effectively leveraged large amounts of unlabeled fault data to enhance model performance. Deng et al. [59] improved HVAC fault identification accuracy by modeling correlations between labeled and unlabeled fault data. Fan et al. [60] designed an HVAC fault diagnosis approach based on graph neural networks. Ma et al. [61] presented a random forest-based semi-supervised method that utilized unlabeled fault data to improve model generalization. Ren et al. [62] designed a semi-supervised method based on the data-pulling strategy to mitigate performance degradation caused by limited labeled samples. Albayati et al. [63] designed an effective semi-supervised method to diagnose rooftop unit faults. SSL methods reduce the dependency on large amounts of labeled training samples. However, these approaches typically rely on sufficient quantities of unlabeled samples to achieve satisfactory results in HVAC fault diagnosis.

As summarized in Table 1, all the aforementioned studies are capable of performing HVAC fault diagnosis experiments with minimal requirements of labeled samples, assuming a sufficient quantity of unlabeled data [64,65]. However, none of the aforementioned studies addresses the issue of HVAC fault diagnosis under the simultaneous scarcity of both labeled and unlabeled data. The above-mentioned problem is particularly prevalent in newly constructed data centers, where both the computing and HVAC systems operate in their new configurations, seeking an energy balance point. While the energy balance cannot be achieved immediately, the HVAC systems may operate at full capacity for an extensive period, increasing the risk of faults. Existing HVAC fault diagnosis methods can hardly be applied to such systems due to the severe shortage of both labeled and unlabeled data. As a result, this study intends to address the HVAC fault diagnosis in data centers with minimal data required. To the best of our knowledge, this is the first study to address HVAC fault diagnosis in data centers with minimal requirements for both labeled and unlabeled data.

1.3. Key challenges and our contribution

As data centers continue to expand rapidly, the automated fault diagnosis of their HVAC systems still faces the following two key challenges:

(1) Scarcity of operational data. Newly constructed data centers have not yet amassed sufficient operational records for chillers and air-handling units. The scarcity of both labeled and unlabeled data severely limits the applicability of data-driven HVAC fault diagnosis models.

(2) Difficulty of labeling. Newly recorded data samples remain largely unlabeled. Manual annotation of fault types and severity levels is prohibitively time-consuming and labor-intensive, preventing the creation of large, high-quality labeled datasets.

To overcome these obstacles, this paper introduces a few-shot semi-supervised learning framework, termed the Semi-Supervised Adaptive Weighted Prototype Network (SSAWPN), specifically tailored for HVAC fault diagnosis in data centers. Few-shot learning by definition deals with the classification tasks with extremely limited data samples. The combination of semi-supervised learning and few-shot learning intends to learn classification tasks with minimal required data, tackling the HVAC fault diagnosis problem in newly built data centers. The learning tasks assign class prototypes to the unlabeled data. The prototypes will be iteratively updated through new HVAC operational data recorded in the data center, with adaptive weights assigned. In summary, the key contributions of our approach are:

(1) Multi-Scale Attention Feature Fusion Network (MSAFN). Designed for newly commissioned data center HVAC systems with virtually no historical data records, MSAFN employs channel-wise segmentation, residual connections, and an attention mechanism to learn fault signatures across multiple spatial and temporal scales. This allows the model to distill the most informative features from limited operational data immediately after system deployment.

(2) Semi-Supervised Adaptive Weighted Prototype Strategy (SAWPS). Tailored to the early-stage operation of data centers, where labeled faults are absent and only a handful of unlabeled anomalies exist, SAWPS incrementally updates class prototypes by assigning adaptive weights to these unlabeled instances. As new data accumulate, prototypes become increasingly representative of real fault modes without requiring manual annotation.

(3) SSAWPN Framework. By integrating MSAFN's multi-resolution feature embeddings with SAWPS's prototype refinement under a meta-learning regime, SSAWPN delivers reliable automated fault diagnosis from day one of a data center's operation. This end-to-end framework ensures high diagnostic accuracy in few-shot scenarios characteristic of newly built HVAC installations.

The remainder of this paper is organized as follows. The relevant theoretical knowledge is introduced in Section 2. Section 3 is devoted to the specific details of the proposed method, including the fault diagnosis framework, the feature extraction network, and the semi-supervised adaptive weighted prototype optimization strategy. The verification experiment and corresponding results analysis are presented in Section 4. Section 5 outlines the conclusions and future research work.

2. Theoretical knowledge

2.1. Semi-supervised few-shot learning

Few-shot learning is commonly applied to classification tasks with extremely limited training samples, which learns category distribution features from a minimal number of data samples and demonstrates strong generalization performance [66]. Different from the traditional supervised learning methods, few-shot learning divides the learning process into multiple tasks, continuously improving the learning ability of the method in the episodic training mode, and enhancing the generalization performance of the network model. The episodic training set D_{TR} is split into a support set S and a query set Q during the training process. A classification problem in few-shot learning with K classes in the support set S, each containing N samples, is known as a K-way N-shot task [67]. A task in few-shot classification is formed by combining the support set S and the query set Q, serving as the fundamental learning unit. In the K-way N-shot paradigm, N instances are randomly sampled from each class to construct a task. This task generation strategy facilitates the creation of diverse learning scenarios, which significantly strengthens the model's capacity for rapid adaptation to new tasks. The mathematical expressions for S and Q are as follows:

$$S = \left\{ \left(x_{k,i}, y_{k,i} \right) \right\}, k = 1, 2, \ldots, K; i = 1, 2, \ldots, n_S \tag{1}$$

$$Q = \left\{ \left(x_{k,j}, y_{k,j} \right) \right\}, k = 1, 2, \ldots, K; j = 1, 2, \ldots, n_Q \tag{2}$$

where $x_{k,\,i}$ and $y_{k,\,i}$ denote the i-th data and label of the k-th category in S, respectively. $x_{k,\,j}$ and $y_{k,\,j}$ refer to the j-th data and label of the k-th category in Q, respectively. n_S and n_Q denote the number of samples of each category in the S and Q, respectively [68].

2.2. Prototypical network

Prototype network (PN) [69], as a representative metric-based few-shot learning method, takes the average value of each category feature vector in the support set as the prototype and claims the prototype as the class center. The predicted probability of a query sample is computed based on its Euclidean distance to the corresponding class prototype.

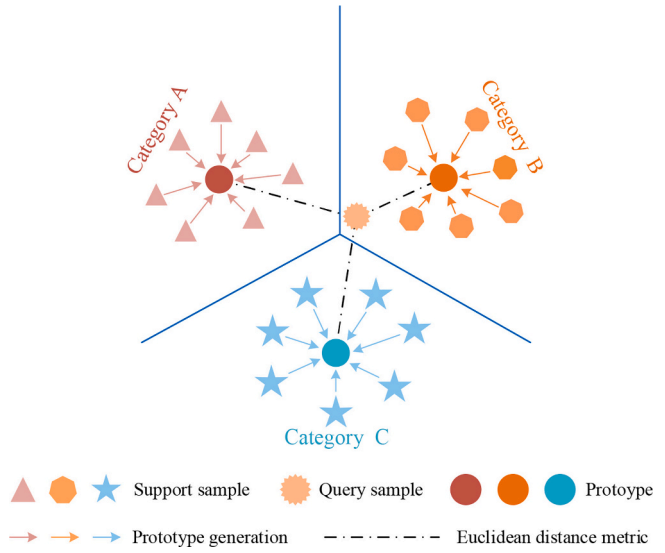

Fig. 1. The schematic representation of the PN.

The category of the sample is determined based on this probability. The classification principle of PN is shown in Fig. 1, including the following implementation steps.

First, a feature extraction network is employed to transform the equipment operational samples into feature vectors of the metric space. The prototype network derives a class prototype by averaging the feature vectors within each category. The prototype for each class is computed as follows:

$$P_a = \frac{1}{n_a}\sum_{i=1}^{n_a} h(x_{a,i}) \tag{3}$$

where P_a represents the prototype of category a. n_a denotes the sample number of category a in S. $x_{a,\,i}$ refers to the i-th sample of class a. $h(\cdot)$ is the feature extraction function.

Second, the probability of a query sample is obtained by measuring the spatial distance between its feature vector and the class prototypes:

$$p(y=a|x_{a,i}\in Q) = \frac{\exp\{-D_E[h(x_{a,i}),P_a]\}}{\sum_{i=1}^{n_Q}\exp\{-D_E[h(x_{a,i}),P_a]\}} \tag{4}$$

where $D_E[.]$ denotes the square of the Euclidean distance.

Lastly, the prototype network (PN) minimizes the average negative log-probability of the query samples as its loss function. Parameter updates are performed iteratively to achieve optimal performance. The loss function is formally defined in Eq. (5).

$$F_{loss} = -\frac{1}{n_Q}\sum_{i=1}^{n_Q}\log p(y=a|x_{a,i}\in Q) \tag{5}$$

2.3. Attention mechanism

The squeeze-excitation attention module (SEM) [70] obtains the global information of input features by optimizing channel-wise representations. It performs squeeze-excitation operations along the channel direction to effectively obtain the channel relationship between features, thereby enhancing the representation of feature vectors (Fig. 2).

The global feature vector representation is extracted from the input features employing a global average pooling (GAP) layer. Subsequently, two fully connected (FC) layers and a nonlinear transformation layer are used to compute the weight information of each feature channel. The channel weights are multiplied with the input features to realize the enhanced representation of feature information. The process can be described in Eqs. (6) and (7) as follows.

$$f_{O1} = f_{\mathrm{ReLU}}(f_{\mathrm{FC}}(f_{\mathrm{GAP}}(x))) \tag{6}$$

$$f_{O2} = f_{\mathrm{Sigmoid}}(f_{\mathrm{FC}}(f_{O1}))*x \tag{7}$$

where $f_{\mathrm{GAP}}(.)$ is the GAP layer operation. $f_{\mathrm{FC}}(.)$ is the FC layer. $f_{\mathrm{ReLU}}(.)$ and $f_{\mathrm{Sigmoild}}(.)$ represent the activation functions ReLU and Sigmoid, respectively.

3. The proposed method

3.1. Fault diagnosis framework

Before the operation data of the HVAC systems is fed into the diagnostic model, the max-min normalization approach is applied to preprocess the original data to speed up the convergence of the model (Eq. 8).

$$x^{\mathrm{ne}} = \frac{x - x_{\min}}{x^{\max} - x_{\min}} \tag{8}$$

Combining the advantages of MSAFN and SAWPS, a HVAC fault diagnosis framework is proposed for newly constructed data centers. The framework is designed to effectively address the challenge posed by the lack of both labeled and unlabeled operational data. The overall implementation process of the diagnostic framework is shown in Fig. 3.

The fault diagnosis framework for data center HVAC systems is designed to follow four main steps:

Step 1: Data acquisition and processing. The operational data of different health states of the HVAC systems are collected, then divided into the support set and query set, and the K-way N-shot paradigm is constructed. For model training, the support set contains a mix of labeled and unlabeled fault samples, while the query set serves to evaluate the diagnostic accuracy of the model.

Step 2: The feature extraction process, outlined in Section 3.2. A channel segmentation and fusion strategy, attention mechanism, and residual connections are incorporated into the architecture of the feature extraction network, forming the MSAFN. MSAFN is employed to capture multi-scale feature information from HVAC system data, thereby enhancing feature representation. The features learned by

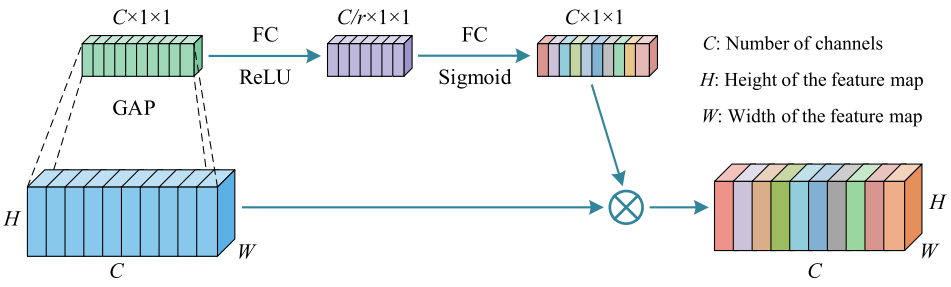

Fig. 2. The structure of the SEM.

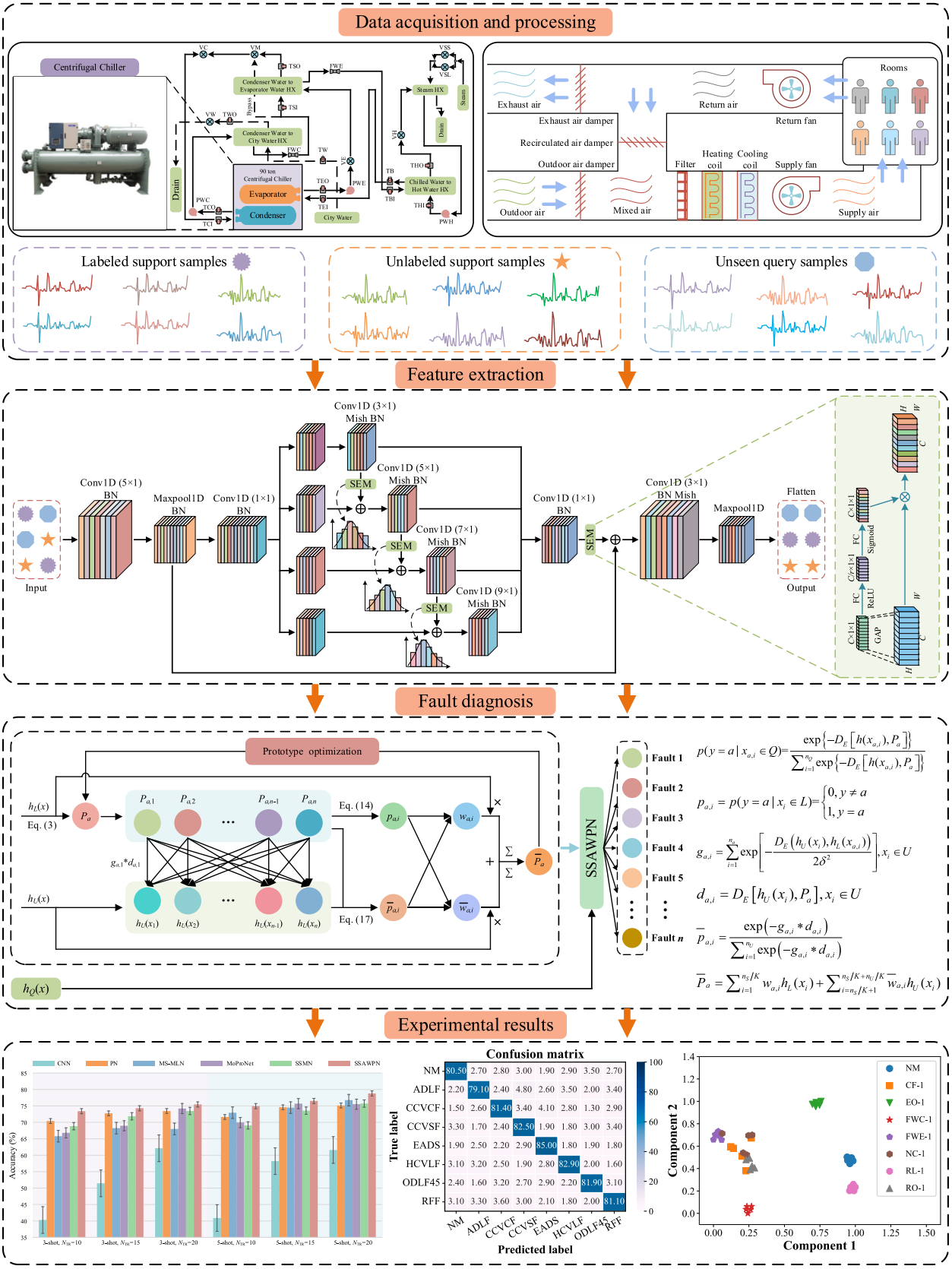

Fig. 3. The proposed data center HVAC systems fault diagnosis framework.

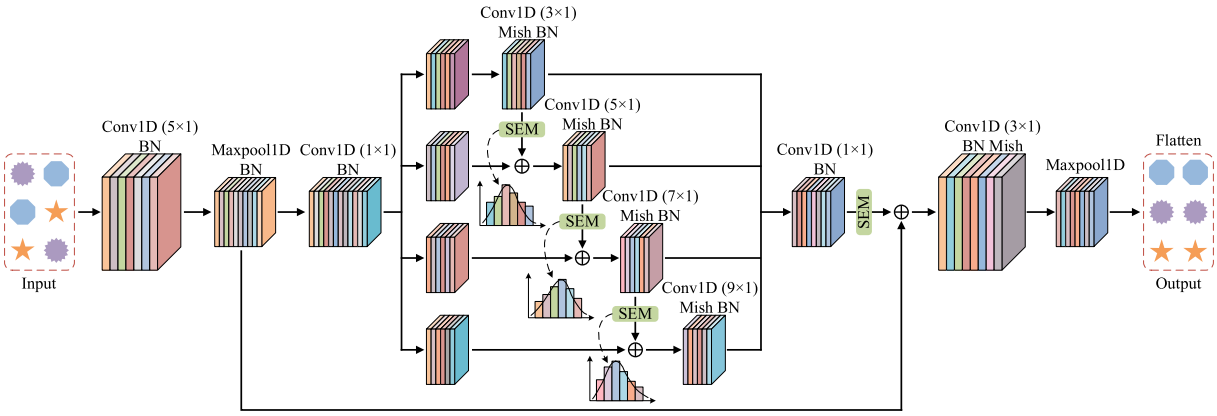

Fig. 4. Schematic of the structure of MSAFN.

MSAFN are transformed into high-dimensional space vector representations for PN.

Step 3: Prototype optimization and fault diagnosis, as demonstrated in Section 3.3. The initial prototype of each fault class is first generated from the feature vector of the labeled fault samples. The prototype is then optimized using the unlabeled fault samples to enhance its quality. Last, the SSAWPN model classifies a query sample by computing its distance to the refined prototypes.

Step 4: Experimental results analysis, as detailed in Section 4. Various evaluation metrics, including accuracy, F1-score, confusion matrix, and t-SNE, are employed to comprehensively evaluate the fault diagnosis capacity of SSAWPN under the condition of limited fault samples for HVAC systems.

3.2. Multi-scale attentive feature fusion network

To effectively learn the different scale information of the fault samples, a multi-scale attentive feature fusion network (MSAFN) is developed to extract the features of the HVAC systems data. MSAFN primarily consists of multiple convolutional layers, max pooling layers, multi-scale feature fusion modules, and a flatten layer. The detailed structure is illustrated in Fig. 4. First, the one-dimensional operational features of the HVAC systems are extracted through a 5 × 1 kernel convolution layer. The batch normalization (BN) operation is applied to mitigate the possibility of the feature distribution shift and enhance the stability of the network. After the data is extracted through a max pooling layer, the feature F is obtained:

$$F = f_{\text{MaxPool}}\left[f_{\text{BN}}\left(f_{\text{Conv}}(x)\right)\right] \tag{9}$$

where x denotes the input data. $f_{\text{Conv}}(.)$ is the convolution operation. $f_{\text{BN}}(.)$ denotes the batch normalization. $f_{\text{MaxPool}}(.)$ represents the max pooling layer.

Subsequently, a convolutional layer with a small kernel is applied to further extract features from F and double the channel dimension, producing the feature F_s. The feature F_s is then split into four parts along the channel dimension, with each part represented as F_i, where $i \in [1–4]$. A convolutional layer, a BN layer, and a Mish activation function are applied in each branch. On the four branches, convolution layers with convolution kernel sizes of 3, 5, 7, and 9 are utilized to extract features of different scales of input samples. Notably, the feature output from the previous branch is enhanced using SEM and then incorporated into the input of the current branch, enabling efficient feature fusion. The mathematical formulation for this process is presented by Eq. (10).

$$E_i = \begin{cases} f_{\text{Mish}}\left[f_{\text{BN}}\left(f_{\text{Conv}}(F_i)\right)\right], & i = 1, \\ f_{\text{Mish}}\left\{f_{\text{BN}}\left[f_{\text{Conv}}\left(F_i + f_{\text{SEM}}(E_{i-1})\right)\right]\right\}, & 2 \le i \le 4. \end{cases} \tag{10}$$

where $f_{\text{Mish}}(.)$ denotes the Mish activation function operation and $f_{\text{SEM}}(.)$ represents the SEM operation.

After fusing the features from each branch, a convolutional layer with a small kernel is employed to further extract the fused features, resulting in a better feature vector representation. The feature output is then obtained using a residual connection, as shown:

$$F_M = F + f_{\text{SEM}}\left\{f_{\text{BN}}\left[f_{\text{Conv}}\left(f_{\text{Ca}}(E_1, E_2, E_3, E_4)\right)\right]\right\} \tag{11}$$

where $f_{\text{Ca}}(.)$ denotes the feature combination operation.

Lastly, the features of F_M are processed through a 3 × 1 kernel convolutional layer followed by a max-pooling layer, and then flattened to obtain the feature vector representation of each data, as follows:

$$F_{\text{out}} = f_{\text{Flateen}}\left\{f_{\text{MaxPool}}\left[f_{\text{BN,Mish}}\left(f_{\text{Conv}}(F_M)\right)\right]\right\} \tag{12}$$

where $f_{\text{Flatten}}(.)$ denotes the feature flattening operation.

Taking the one-dimensional chiller data with 64 features from the RP1043 project as an example, Table 2 presents a detailed layer-by-layer description of how the data is progressively transformed within the MSAFN model.

Table 2
Architecture of the MSAFN model.

ID	Layer	Input shape	Output shape	ID	Layer	Input shape	Output shape
1	Conv1D (5 × 1)	(1, 64)	(128, 62)	12	BN, Mish	(64, 15)	(64, 15)
2	BN	(128, 62)	(128, 62)	13	Conv1D (9 × 1)	(64, 15)	(64, 15)
3	Maxpool1D	(128, 62)	(128, 15)	14	BN, Mish	(64, 15)	(64, 15)
4	BN	(128, 15)	(128, 15)	15	Conv1D (1 × 1)	(256, 15)	(128, 15)
5	Conv1D (1 × 1)	(128, 15)	(256, 15)	16	BN	(128, 15)	(128, 15)
6	BN	(256, 15)	(256, 15)	17	SEM	(128, 15)	(128, 15)
7	Conv1D (3 × 1)	(64, 15)	(64, 15)	18	Residual connection	(128, 15)	(128, 15)
8	BN, Mish	(64, 15)	(64, 15)	19	Conv1D (3 × 1)	(128, 15)	(128, 15)
9	Conv1D (5 × 1)	(64, 15)	(64, 15)	20	BN, Mish	(128, 15)	(128, 15)
10	BN, Mish	(64, 15)	(64, 15)	21	Maxpool1D	(128, 15)	(128, 7)
11	Conv1D (7 × 1)	(64, 15)	(64, 15)	22	Flatten	(128, 7)	(896)

$$\overline{P}_a = \sum_{i=1}^{n_S/K} w_{a,i} h_L(x_i) + \sum_{i=n_S/K+1}^{n_S/K+n_U/K} \overline{w}_{a,i} h_U(x_i) \tag{20}$$

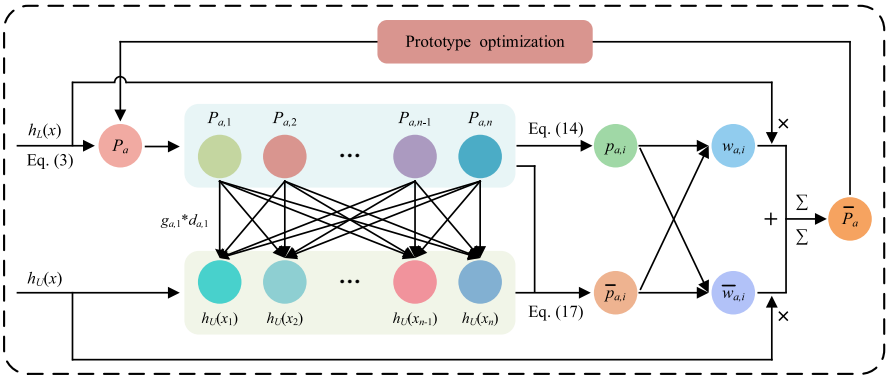

Fig. 5. Schematic of SAWPS.

Fig. 5. Schematic of SAWPS.

3.3. Semi-supervised adaptive weighted prototype optimization strategy

The prototype serves as an important basis for classification tasks, and its quality has a key impact on the overall experimental outcomes. To alleviate the impact of the limited labeled fault samples in the support set on the prototype location, and to obtain higher quality prototypes that enhance the diagnostic capability of the fault diagnosis framework, a semi-supervised adaptive weighted prototype optimization strategy is proposed. SAWPS fully leverages the information from unlabeled fault data to optimize the original prototype of each category, and its schematic diagram is illustrated in Fig. 5. A summary of the main idea of SAWPS is presented below.

First, this study incorporates unlabeled samples into the support set, which necessitates a revised definition as follows.

$$S = L \cup U = \{(x_i, y_i)\}_{i=1}^{n_L} \cup \{(x_i)\}_{i=n_L}^{n_L+n_U} \tag{13}$$

where L and U denote the labeled and unlabeled datasets, respectively. n_L and n_U indicate the sample counts of the labeled and unlabeled datasets, respectively.

MSAFN is employed to transform the input data from the support set into spatial vector representations. The spatial feature representations of the labeled and unlabeled samples are presented as $h_L(x)$ and $h_U(x)$, respectively. The initial prototype for each labeled category in the support set is computed using Eq. (3). Subsequently, probability assignment for the labeled samples of each category is performed as follows:

$$p_{a,i} = p(y = a | x_i \in L) = \begin{cases} 0, y \neq a \\ 1, y = a \end{cases} \tag{14}$$

Second, the distance from each unlabeled sample to the initial prototype is computed. The sum of the Gaussian kernel similarity matrix of each unlabeled sample and all labeled samples of the category is computed as the weight matrix, as shown in Eq. (15). The δ is the scaling factor, and its value will be discussed in Section 4.2. The weight matrix is incorporated into the probability calculation of unlabeled samples, which makes the probability assignment of unlabeled samples more accurate. The process is described in Eqs. (16) and (17).

$$g_{a,i} = \sum_{i=1}^{n_a} \exp\left[-\frac{D_E\left(h_U(x_i), h_L\left(x_{a,i}\right)\right)}{2\delta^2} \right], x_i \in U \tag{15}$$

$$d_{a,i} = D_E[h_U(x_i), P_a], x_i \in U \tag{16}$$

$$\overline{p}_{a,i} = \frac{\exp\left(-g_{a,i} * d_{a,i}\right)}{\sum_{i=1}^{n_U} \exp\left(-g_{a,i} * d_{a,i}\right)} \tag{17}$$

where $D_E(.)$ denotes the square of Euclidean distance, and $g_{a,i}$ represents the weight matrix corresponding to the case where the i-th data sample in the unlabeled sample set is classified into class a.

Lastly, to optimize the position of the initial prototype, the probability of labeled samples and unlabeled samples in the support set is converted into the coefficient, and two weight coefficients related to the data class are obtained. The weight coefficients are embedded into the update process of the prototype to generate the new prototype, as shown in Eqs. (18) to (20):

$$w_{a,i} = \frac{p_{a,i}}{\sum_{i=1} p_{a,i} + \sum_{j=1} \overline{p}_{a,j}} \tag{18}$$

$$\overline{w}_{a,i} = \frac{\overline{p}_{a,i}}{\sum_{i=1} p_{a,i} + \sum_{j=1} \overline{p}_{a,j}} \tag{19}$$

$$\overline{P}_a = \sum_{i=1}^{n_S/K} w_{a,i} h_L(x_i) + \sum_{i=n_S/K+1}^{n_S/K+n_U/K} \overline{w}_{a,i} h_U(x_i) \tag{20}$$

4. Experiments and result analysis

The diagnostic framework developed is constructed based on the PyTorch learning platform in this study. During the model training, the stochastic gradient descent optimizer is employed, with an initial learning rate of 0.1 and a momentum of 0.96. An exponential decay strategy is utilized to update the learning rate, with the number of training iterations fixed at 30. The reported results are based on the average of ten independent experiments to enhance their statistical reliability.

To demonstrate the superiority of SSAWPN in few-shot scenarios, recently published semi-supervised or few-shot learning methods are selected in the comparative study. The compared baseline models include the conventional semi-supervised meta-network (SSMN) [67], the adaptive convolutional neural network (CNN) [71], the prototype network (PN) [69], the multi-scale meta-learning network (MS-MLN) [72], and the momentum prototypical neural network (MoProNet) [73]. The SSMN [67] (Feng et al., 2022) is a classic semi-supervised learning-based fault diagnosis framework, which uses unlabeled fault samples to optimize the location of prototypes to obtain better classification results. The adaptive CNN [71] (Yan et al., 2022) is a semi-supervised convolutional neural network model used for chiller fault diagnosis. PN [67] is a basic few-shot network. MS-MLN [72] (Wang and Liu, 2024) is

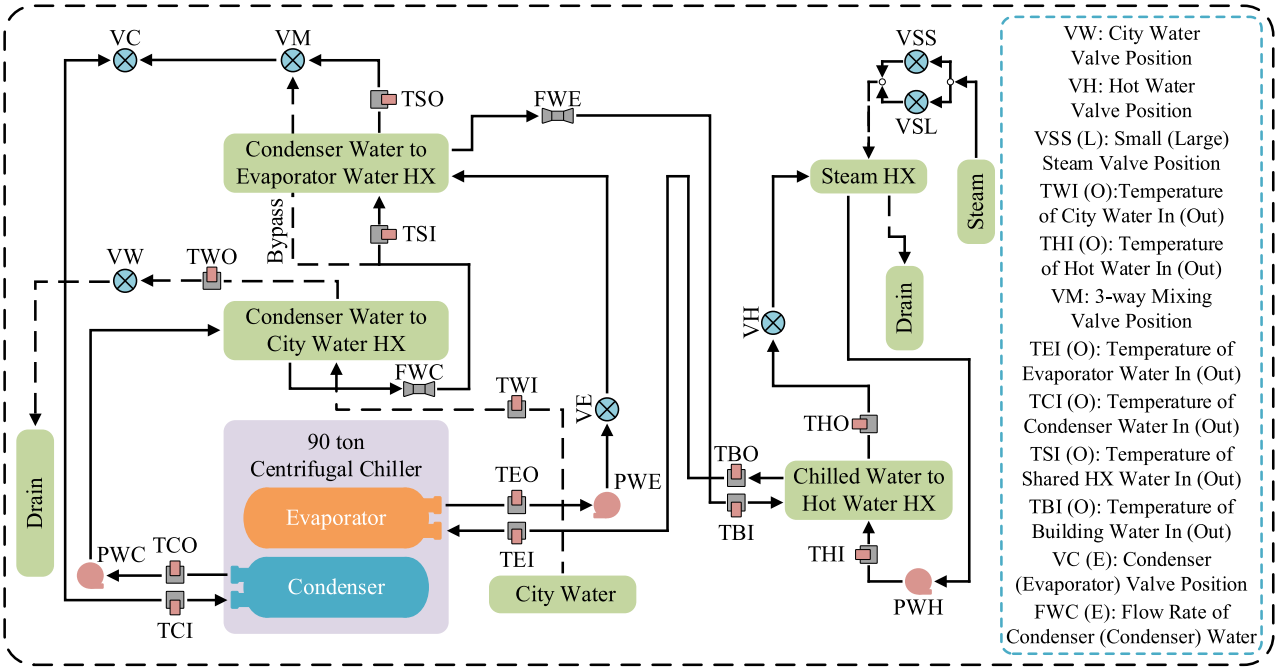

Fig. 6. Schematic diagram of the chiller test device [76].

Table 3
The details of each SL.

Health conditions	SL1		SL2		SL3		SL4	
	Bias	Label	Bias	Label	Bias	Label	Bias	Label
NM	0	NM	0	NM	0	NM	0	NM
CF	−12 %	CF-1	−20 %	CF-2	−30 %	CF-3	−45 %	CF-4
EO	+14 %	EO-1	+32 %	EO-2	+50 %	EO-3	+68 %	EO-4
FWC	−10 %	FWC-1	−20 %	FWC-2	−30 %	FWC-3	−40 %	FWC-4
FWE	−10 %	FWE-1	−20 %	FWE-2	−30 %	FWE-3	−40 %	FWE-4
NC	+1 %	NC-1	+2 %	NC-2	+3 %	NC-3	+5 %	NC-4
RL	−10 %	RL-1	−20 %	RL-2	−30 %	RL-3	−40 %	RL-4
RO	+10 %	RO-1	+20 %	RO-2	+30 %	RO-3	+40 %	RO-4

a meta learning network model for cross-domain fault diagnosis. MS-MLN utilizes a multi-branch feature fusion strategy to capture multi-scale features from limited available data. MoProNet [73] (Chen et al., 2024) is a prototype neural network model designed for rotating machinery. MoProNet utilizes convolution kernels of varying sizes to extract features at multiple scales and optimizes the training parameters of the model.

Accuracy and F1-score are widely adopted evaluation metrics for assessing the effectiveness of deep learning models in fault diagnosis tasks. The specific mathematical expressions are provided in Eqs. (21) and (22), respectively. The number of true positive (TP), true negative (TN), false positive (FP), and false negative (FN) samples is utilized for the evaluation. Additionally, to visually present the experimental results of each method, the confusion matrix [74] and t-SNE [75] visualization techniques are employed.

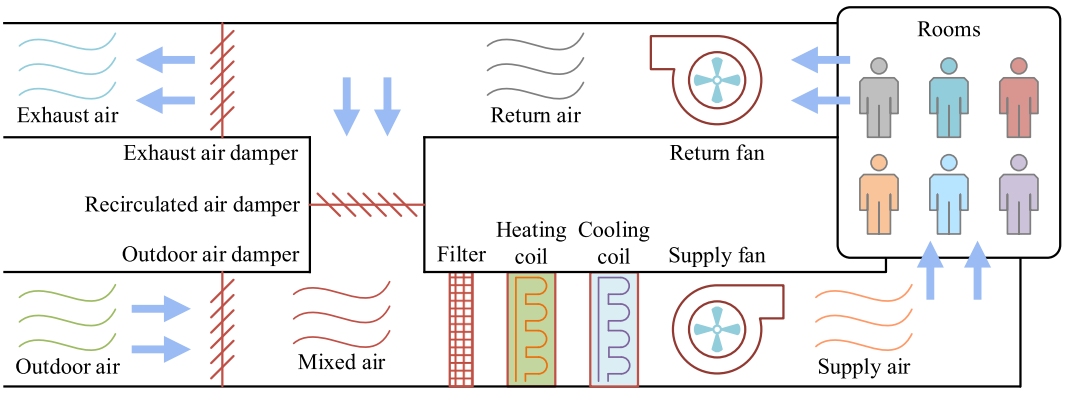

Fig. 7. Schematic diagram of the AHU test device [77].

Table 4
Details of AHU datasets.

Summer			Winter	
Index	Fault type	Label	Fault type	Label
1	Normal	NM	Normal	NM
2	AHU duct leaking fault (after supply) fan	ADLF	Cooling coil valve stuck fault (20 % open)	CCVSF
3	Cooling coil valve control fault (unstable)	CCVCF	Exhaust air damper stuck (fully closed)	EADSFC
4	Cooling coil valve stuck fault (15 % open)	CCVSF	Exhaust air damper stuck (fully open)	EADSFO
5	Exhausted air damper stuck (fully open)	EADS	Heating coil fouling fault	HCFF
6	Heating coil valve leaking fault (0.4 GPM)	HCVLF	Heating coil reduced capacity	HCRC
7	Outdoor air damper leaking fault (45 % open)	ODLF45	Outdoor air damper leaking fault (52 % open)	OADLF
8	Return fan fault (fixed speed)	RFF	Outdoor air damper stuck fault (fully closed)	OADSF

Table 5
The features selected from the AHU datasets.

Index	Feature type	Index	Feature type
1	Supply air temperature	11	Outdoor air flow rate
2	Return air temperature	12	Heating coil energy consumption
3	Cooling coil load	13	Return fan energy consumption
4	Return air humidity	14	Outside air damper temperature
5	Supply air humidity	15	Supply fan speed
6	Mixed air temperature	16	Return fan speed
7	Chilled water coil discharge air temperature	17	Supply air duct static pressure
8	Supply fan energy consumption	18	Differential pressure of supply air fan (Pa)
9	Supply air flow rate	19	Differential pressure of return air fan (Pa)
10	Return air flow rate		

$$\text{Accuracy} = \frac{TP + TN}{TP + FP + TN + FN} \tag{21}$$

$$\text{F1} = \frac{2TP}{2TP + FP + FN} \tag{22}$$

4.1. Dataset details

4.1.1. Dataset one: Chiller fault dataset

In this dataset, the operational data from the ASHRAE project 1043-RP [76] are employed to verify the effectiveness and superiority of SSAWPN. The test system of the project is illustrated in Fig. 6. Based on fault occurrence rates, the project simulates seven representative faults that may arise during the operation of a centrifugal chiller. A total of eight health conditions are considered, including normal (NM), reduced condenser water flow (FWC), reduced evaporator water flow (FWE), refrigerant leakage (RL), refrigerant overcharge (RO), excess oil (EO), condenser fouling (CF), and non-condensable in refrigerant (NC). During the experiments, 64 characteristic variables such as temperature, flow rate, and power of the chiller operation are recorded using multiple groups of sensors. All faults are classified into four distinct severity levels (SL), namely SL1 through SL4. The detailed biases of all four severity levels are listed in Table 3. To simulate the scenario of scarce fault samples, 60 samples are randomly selected for each fault type (including the normal type) and each severity level from the data collected by the ASHRAE 1043-RP project for model training and testing.

Table 6
The accuracy of SSAWPN in different N_U.

Datasets	N_U for 5-shot (%)					
	0	1	2	3	4	5
Dataset one (SL1)	71.63 ± 1.18	**74.57** ± 2.36	74.10 ± 1.87	72.57 ± 2.71	72.42 ± 1.26	73.17 ± 1.51
Dataset two (summer)	68.69 ± 1.62	**71.61** ± 0.71	71.26 ± 0.77	70.78 ± 0.96	70.72 ± 1.26	70.16 ± 1.37
Sum	140.32	**146.18**	145.36	143.35	143.14	143.33

4.1.2. Dataset two: AHU fault dataset

Derived from the ASHRAE 1312-RP project, the AHU datasets are utilized in this study, with the main structure of the experimental setup depicted in Fig. 7. In this project, two identical AHUs (AHU-A and AHU-B) are employed, with AHU-A simulating various possible failures and AHU-B operating normally. The AHU fault data are collected during summer, winter, and spring, and more details can be found in [77]. Both summer and winter datasets are applied to assess the diagnostic capability of the framework. For each season, seven typical fault samples and normal samples are employed to construct the summer and winter datasets, as summarized in Table 4. Moreover, 19 commonly used features are selected according to the literature [78,79], and the details are provided in Table 5. Similarly, to simulate a limited-data scenario for AHU systems, 60 samples are randomly selected for each health condition.

4.2. Ablation experiments

4.2.1. Parametric ablation experiments

To determine the optimal number of unlabeled fault samples for prototype optimization, varying quantities of unlabeled fault samples are employed during experimentation. Specifically, the quantity of labeled fault data drawn from each fault class is denoted as N_{TR}. In this experiment, the value of δ is set to 1.0. The number of unlabeled fault samples (N_U) in each fault class of the support set varies from 0 to 5. The number of labeled fault samples in each category is set to 5. Additionally, the size of N_{TR} is set to 10. Ten independent repeated experiments are performed to compare the average accuracy of dataset one (SL1) and dataset two (summer) under different values of N_U. Table 6 summarizes the experimental results, and the best-performing values are highlighted in bold.

Table 6 demonstrates that the accuracy of SSAWPN on dataset one (SL1) initially improves and then decreases as the quantity of unlabeled fault data increases. The best accuracy (74.57 %) is achieved when the value of N_U is set to one, which is 2.94 % higher than the accuracy (71.63 %) obtained without using unlabeled fault samples. A similar trend is observed in dataset two (summer), where the accuracy first improves and then declines as N_U increases, indicating that a reasonable number of unlabeled fault samples can significantly enhance the diagnostic performance of SSAWPN. In dataset two (summer), using one unlabeled fault sample per category obtains the most significant improvement on the accuracy of SSAWPN, with a 2.92 % increase over the accuracy (68.69 %) obtained without any unlabeled fault samples. Moreover, incorporating unlabeled fault samples leads to higher diagnostic accuracy compared to approaches that rely solely on labeled data. Comprehensive analysis shows that using one unlabeled fault sample per class to optimize the prototype can obtain the best diagnosis performance. Therefore, the quantity of unlabeled fault data for each health state is set to one in this study.

To determine the effective value of the scaling factor δ in SAWPS, the value of δ is set from 0.1 to 1.0 in the 5-shot experiment. In this

Table 7
The accuracy of SSAWPN in different δ.

Datasets	δ for 5-shot (%)									
	0.1	0.2	0.3	0.4	0.5	0.6	0.7	0.8	0.9	1.0
Dataset one (SL1)	73.09 ± 1.88	74.38 ± 3.01	73.78 ± 1.16	73.96 ± 2.64	73.60 ± 1.33	73.71 ± 2.46	74.08 ± 2.53	**74.95** ± 2.80	73.91 ± 2.47	74.57 ± 2.36
Dataset two (summer)	71.73 ± 0.45	71.56 ± 1.01	71.64 ± 0.58	**72.09** ± 1.17	71.88 ± 0.66	72.02 ± 0.72	71.74 ± 0.81	71.80 ± 0.39	71.90 ± 0.66	71.61 ± 0.71
Sum	144.82	145.94	145.42	146.05	145.48	145.73	145.82	**146.75**	145.81	146.18

Table 8
The average accuracy of each method on dataset one (SL1).

Methods	N_{TR} for 3-shot (%)			N_{TR} for 5-shot (%)			Average
	10	15	20	10	15	20	
Method 1	70.41 ± 1.23	72.75 ± 0.85	73.45 ± 0.62	71.63 ± 1.18	74.59 ± 1.38	75.14 ± 1.36	73.00
Method 2	70.98 ± 1.65	73.82 ± 1.35	73.96 ± 1.34	74.12 ± 2.69	75.79 ± 1.41	76.78 ± 2.47	74.24
Method 3	71.56 ± 1.25	73.77 ± 0.90	74.03 ± 0.84	71.91 ± 1.35	74.72 ± 0.78	76.13 ± 1.08	73.69
Method 4	**73.40** ± 1.05	**74.28** ± 1.99	**75.46** ± 0.81	**74.95** ± 2.80	**76.52** ± 1.05	**78.81** ± 1.37	**75.57**

Table 9
The average accuracy of each method on dataset two (summer).

Methods	N_{TR} for 3-shot (%)			N_{TR} for 5-shot (%)			Average
	10	15	20	10	15	20	
Method 1	65.75 ± 1.52	72.46 ± 1.18	74.96 ± 2.05	68.69 ± 1.62	75.51 ± 1.22	79.33 ± 1.04	72.78
Method 2	69.58 ± 1.44	72.98 ± 1.76	78.21 ± 1.02	71.76 ± 0.62	76.25 ± 0.89	80.39 ± 0.71	74.86
Method 3	67.71 ± 1.39	73.15 ± 1.09	77.25 ± 1.66	69.56 ± 1.13	75.73 ± 1.70	81.00 ± 1.05	74.06
Method 4	**69.66** ± 1.34	**75.50** ± 0.86	**78.38** ± 2.07	**71.80** ± 0.39	**76.57** ± 1.12	**81.19** ± 0.96	**75.52**

experiment, the values of N_U and N_{TR} are set to 1 and 10, respectively. The experiments are carried out with dataset one (SL1) and dataset two (summer). The results are summarized in Table 7, and the best average accuracy is shown in bold.

The experimental results in Table 7 demonstrate that SSAWPN achieves the best experimental results on dataset one (SL1) and dataset two (summer) when the value of δ is set to 0.8 and 0.4, respectively. To determine the best parameters of δ, the sum of the accuracy is calculated for two datasets. The accuracy sum for $\delta = 0.8$ (146.75 %) is 0.57 % and 0.70 % higher than that of the second-best (146.18 %) and third-best (146.05 %) settings, respectively. Based on this comprehensive comparison, $\delta = 0.8$ is selected as the optimal value for this study.

4.2.2. Structural ablation experiments

Referring to the results discussed in Section 4.2.1, the values of N_U and δ are set to 1 and 0.8, respectively. The PN model is utilized as the baseline for comparison in the ablation study, which aims to evaluate the effectiveness of each component within SSAWPN and assess their respective contributions to the diagnostic task. The structural ablation experiment is arranged as follows.

(1) Method 1: PN is used as the comparison baseline of all methods, meaning that MSAFN and SAWPS are not adopted.

(2) Method 2: Simply replace the feature extraction network in PN with MSAFN without employing SAWPS.

(3) Method 3: The prototype network in PN is replaced with SAWPS, without incorporating MSAFN.

(4) Method 4: The SSAWPN, which integrates both MSAFN and SAWPS.

Experiments are conducted on dataset one (SL1) and dataset two (summer), and the value of N_{TR} is set to 10, 15, and 20 for 3-shot and 5-shot experiments, respectively. The experimental results of each method are presented in Tables 8 and 9, and the best experimental results are highlighted in bold.

The results in Table 8 demonstrate that Method 2 achieves significantly higher accuracy than Method 1 in all diagnostic tasks. The average accuracy of Method 2 (74.24 %) in six tasks is 1.24 % higher than that of Method 1 (73.00 %). The findings indicate that the MSAFN is more effective in extracting fault-related features compared to the feature extraction network employed in PN. The accuracy results for Method 3 and Method 1 in the 3-shot and 5-shot diagnostic tasks indicate that the strategy of leveraging unlabeled fault samples to optimize prototypes is generally more effective than the original prototype update strategy. On average, SAWPS achieves 0.69 % higher accuracy across all diagnostic tasks compared to the original update strategy. The results of Methods 2 and 3 show that MSAFN and SAWPS are effective not only in SSAWPN but also in other network structures. Obviously, the accuracy of Method 4 is better than that of the comparison methods in all 3-shot and 5-shot diagnostic tasks. Its average accuracy (75.57 %) is 2.57 %, 1.33 %, and 1.88 % higher than that of Method 1 (73.00 %), Method 2 (74.24 %), and Method 3 (73.69 %), respectively. Similarly, the results in Table 9 show that both SAWPS and MSAFN can improve the diagnostic accuracy of the model, with MSAFN contributing more significantly to the performance improvement of SSAWPN than SAWPS. Method 4 demonstrates the best performance among all methods in the 5-shot tasks, with an average accuracy of 75.52 %, surpassing Method 1 (72.78 %), Method 2 (74.86 %), and Method 3 (74.06 %) by 2.74 %, 0.66 %, and 1.46 %, respectively. Overall, the diagnostic performance of SSAWPN surpasses that of PN, as well as the methods that use either MSAFN or SAWPS individually.

4.3. Comparative experiments

4.3.1. Case one: Few-shot fault diagnosis for chillers

As shown in Table 3, the severity of faults in the chiller system increases progressively from SL1 to SL4, while the corresponding difficulty of fault diagnosis decreases accordingly. Specifically, SL1 typically represents the early stage of the fault or the minor anomaly, where fault characteristics are subtle. Consequently, fault diagnosis under the SL1

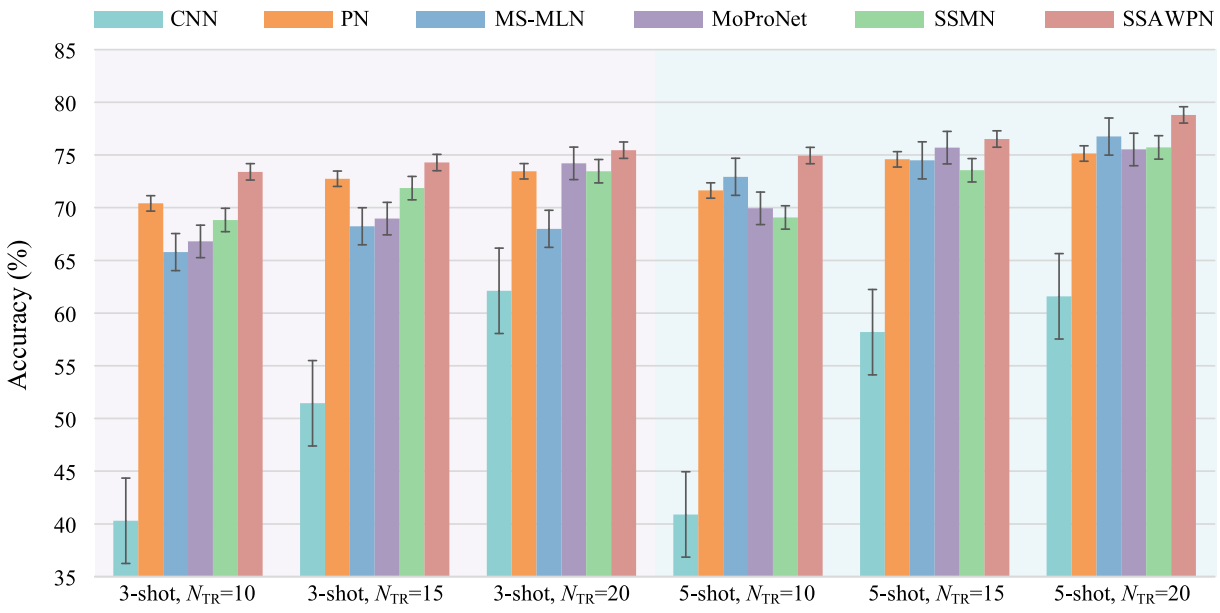

Fig. 8. The accuracy of each method on SL1.

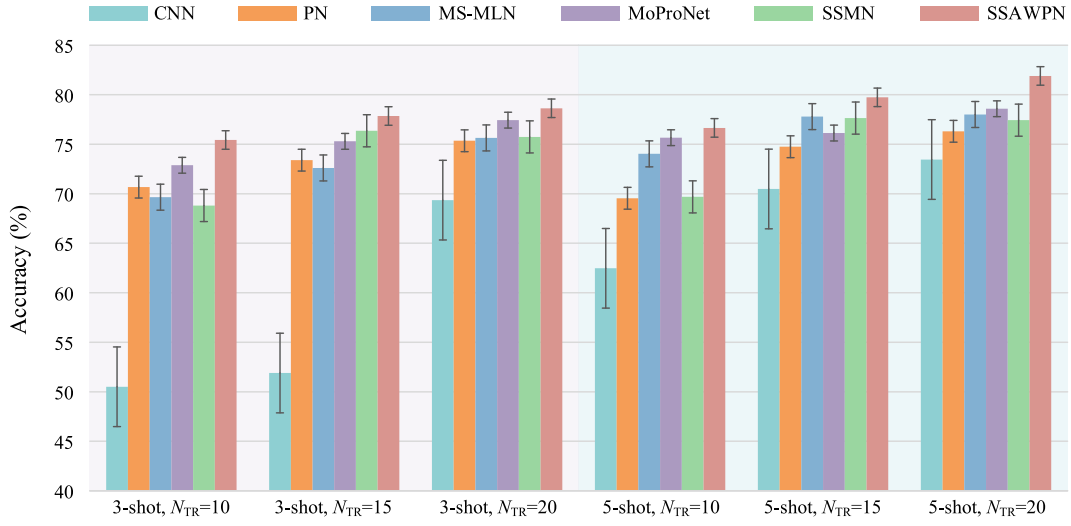

Fig. 9. The accuracy of each method on SL2.

condition imposes greater demands on the framework's feature extraction capability. In contrast, as the fault severity increases from SL2 to SL4, system anomalies become more pronounced, making the diagnosis task relatively easier. To comprehensively assess the adaptability and effectiveness of the developed diagnostic approach under varying fault severity levels, experiments are conducted across all four severity categories (SL1 to SL4).

To simulate fault diagnosis scenarios under limited fault sample conditions, 3-shot and 5-shot fault diagnosis experiments are conducted. During the experiment, the value of N_{TR} is set to 10, 15, and 20, respectively. A total of six types of comparison experiments are carried out for each fault level. The diagnostic results of all methods on SL1, SL2, SL3, and SL4 are detailed in Figs. 8–11, respectively.

Fig. 8 clearly illustrates that the accuracy of CNN in all diagnostic tasks of 3-shot and 5-shot is significantly lower than that of other comparison frameworks. In particular, the maximum performance gap between CNN and SSAWPN reaches 33.11 % and 34.05 % in the 3-shot and 5-shot tasks, respectively. This indicates that CNN struggles to extract sufficient fault features from limited fault data, resulting in suboptimal diagnostic performance. In contrast, PN achieves a substantial improvement in accuracy over CNN across all tasks, with the largest margin reaching 30.73 %. This highlights the advantages of few-shot learning approaches in dealing with limited fault data, as they effectively mitigate the negative impact of insufficient labeled fault samples. While the accuracy of MS-MLN is lower than that of PN in the 3-shot diagnosis task, it outperforms PN in the 5-shot task. The results suggest that the multi-branch feature fusion method of MS-MLN may lead to feature interference when only a few samples are available per class, limiting its generalization ability in few-shot conditions. MoProNet demonstrates significantly higher accuracy than both CNN and MS-MLN in the 3-shot experiments, with the largest accuracy improvements being 29.04 % and 6.21 %, respectively. The results indicate that using convolution kernels of different sizes in MoProNet is beneficial for extracting the fault features of the chillers, thereby enhancing diagnostic performance. SSMN optimizes the prototype by using unlabeled fault samples and achieves better diagnosis results than MS-MLN in the 3-shot diagnosis task, but the accuracy is not ideal in the 5-shot diagnosis task. Overall, SSAWPN significantly outperformed the other five comparison

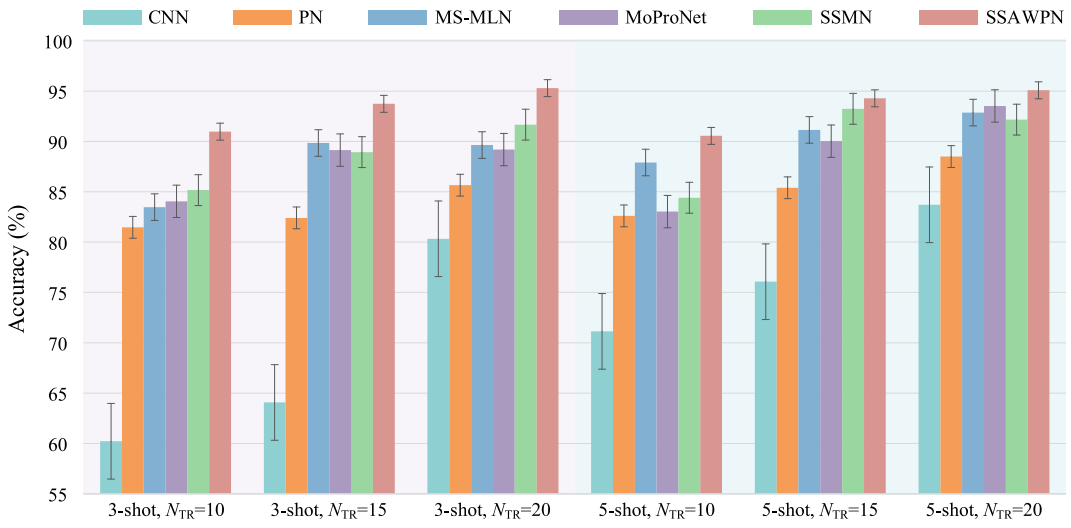

Fig. 10. The accuracy of each method on SL3.

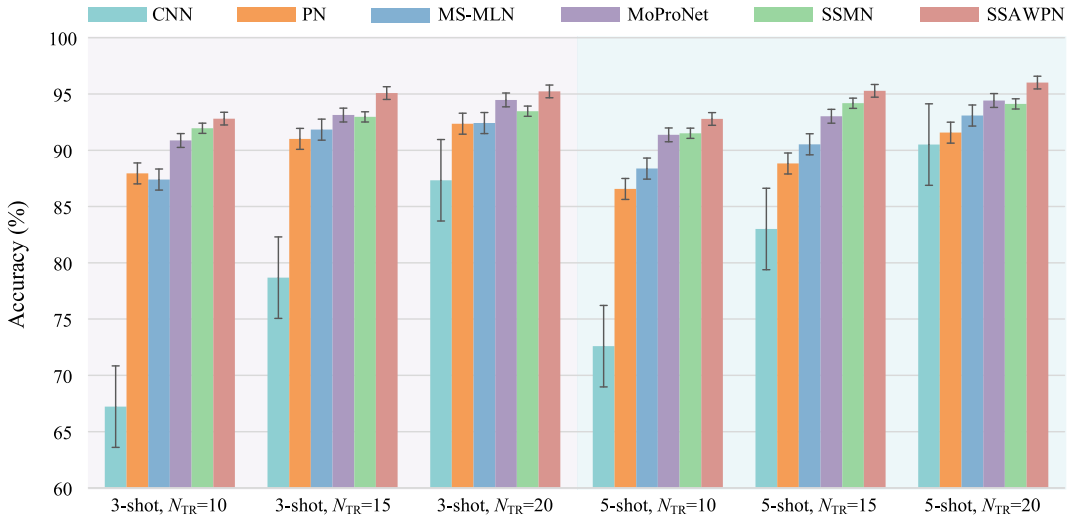

Fig. 11. The accuracy of each method on SL4.

methods in all diagnostic tasks. The maximum accuracy improvements between SSAWPN and CNN, PN, MS-MLN, MoProNet, and SSMN reach 34.05 %, 3.66 %, 7.61 %, 6.60 %, and 5.87 %, respectively. Moreover, the accuracy of the SSAWP remains relatively stable across all tasks, with only minor fluctuations. It demonstrates that SSAWPN with multi-scale attentive feature fusion and the semi-supervised adaptive weighted prototype optimization strategy has significant advantages in scenarios with scarce fault samples, and shows strong generalization performance and robustness.

The results in Figs. 9–11 further highlight the advantage of SSAWPN across varying fault severity levels. In the SL2 diagnosis task, SSAWPN outperforms CNN, PN, MS-MLN, MoProNet, and SSMN by the maximum accuracy margins of 25.96 %, 7.11 %, 5.78 %, 3.61 %, and 6.62 %, respectively. The corresponding average accuracy improvements are 15.34 %, 5.03 %, 3.75 %, 2.37 %, and 4.09 %. Similarly, in the SL3 diagnosis task, SSAWPN achieves the maximum accuracy margins of 30.76 %, 11.33 %, 7.50 %, 7.52 %, and 6.14 % over CNN, PN, MS-MLN, MoProNet, and SSMN, respectively. The average accuracy differences in this task are 20.73 %, 8.98 %, 4.17 %, 5.16 %, and 4.06 %. In the SL4 diagnosis task, the maximum accuracy differences between SSAWPN and CNN, PN, MS-MLN, MoProNet, and SSMN are 25.59 %, 6.46 %, 5.41 %, 2.26 %, and 2.12 %, respectively. The corresponding average

Table 10
The F1 score of each method on dataset one (SL1).

Methods	N_{TR} for 3-shot (%)			N_{TR} for 5-shot (%)			Average
	10	15	20	10	15	20	
CNN	36.30	52.87	61.51	36.73	56.72	62.13	51.04
PN	68.87	71.35	71.81	70.73	73.72	74.30	71.80
MS-MLN	63.63	66.23	66.13	71.18	73.22	75.45	69.31
MoProNet	64.97	67.24	72.52	68.50	74.48	74.21	70.32
SSMN	67.24	69.82	71.79	67.78	72.18	74.56	70.56
SSAWPN	**71.29**	**72.30**	**73.22**	**73.54**	**75.01**	**77.25**	**73.77**

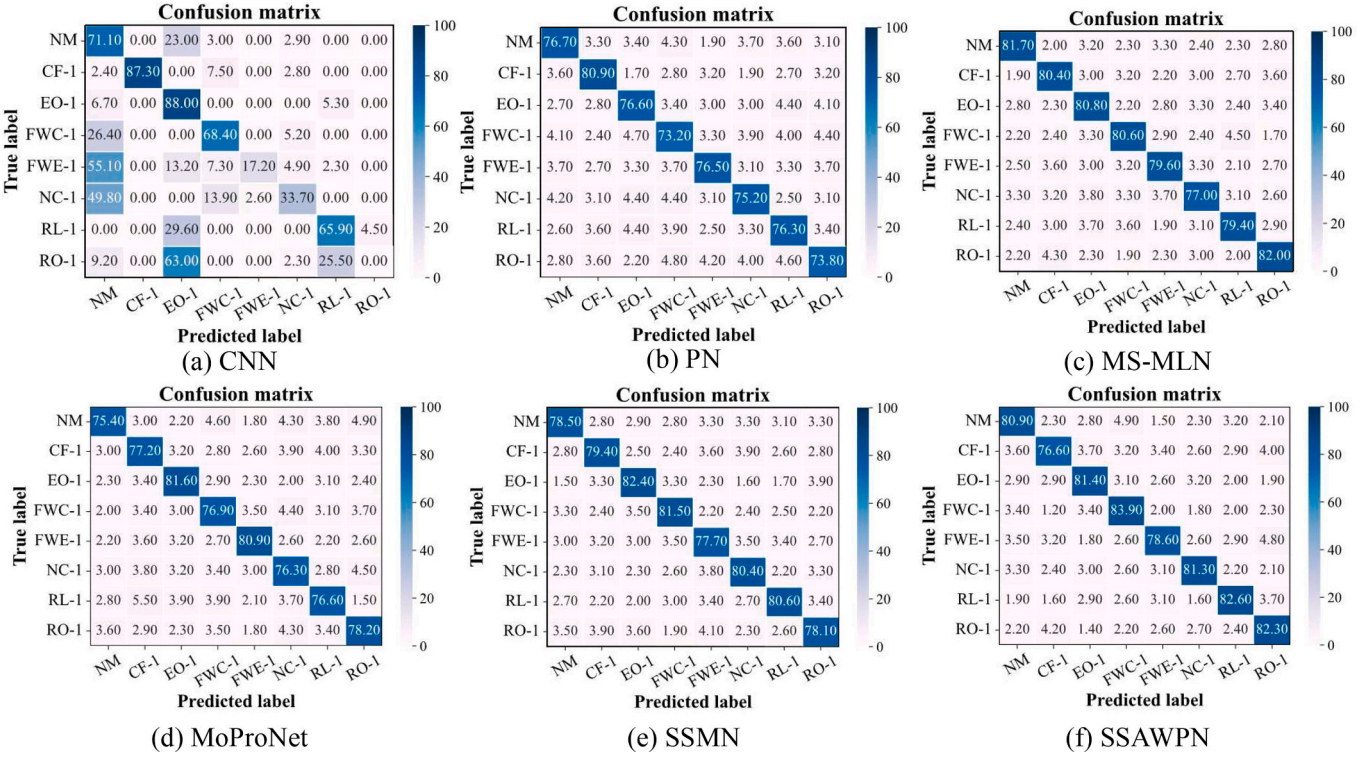

Fig. 12. Confusion matrix results on dataset one (SL1) for the 5-shot task with $N_{TR} = 20$.

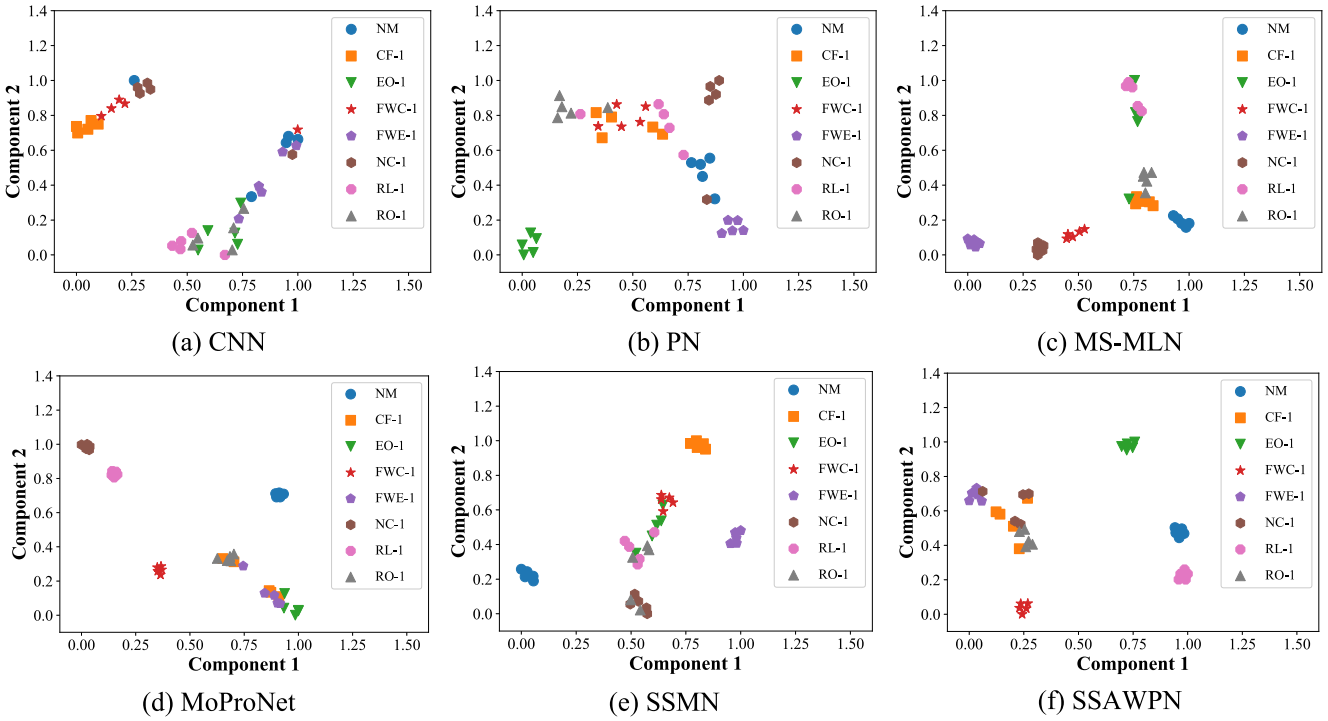

Fig. 13. t-SNE results on dataset one (SL1) for the 5-shot task with $N_{TR} = 20$.

accuracy improvements are 14.64 %, 4.82 %, 3.93 %, 1.65 %, and 1.50 %. Although SSMN employs unlabeled fault samples to optimize class prototypes, its diagnostic accuracy is lower than that of the SSAWPN in all diagnostic tasks. This indicates that SSAWPN is more capable of adapting to a variety of complex few-shot fault diagnosis tasks than SSMN. Overall, SSAWPN significantly outperforms CNN, PN, MS-MLN, MoProNet, and SSMN in average accuracy in all tasks on SL2, SL3, and SL4.

As previously noted, SL1 represents the most challenging fault diagnosis scenario due to its subtle fault characteristics and limited data. Model performance on the SL1 dataset is further evaluated using the F1 score, confusion matrix, and t-SNE visualization. These results provide

Table 11
The F1 score of each method on dataset two (summer).

Methods	N_{TR} for 3-shot (%)			N_{TR} for 5-shot (%)			Average
	10	15	20	10	15	20	
CNN	27.25	39.09	61.05	28.99	41.96	63.90	43.71
PN	63.41	70.71	73.50	67.27	74.51	78.63	64.96
MS-MLN	63.35	69.16	73.01	68.30	73.14	76.32	64.00
MoProNet	63.50	70.53	75.31	68.05	**75.50**	80.06	65.65
SSMN	65.36	71.13	75.50	69.43	74.58	79.63	65.87
SSAWPN	**67.68**	**73.72**	**77.02**	**70.65**	75.39	**80.50**	**67.22**

deeper insight into the classification accuracy, misclassification patterns, and feature distribution of different diagnostic models. The corresponding results are presented in Table 10, Fig. 12, and Fig. 13.

Table 11 shows the experimental results of the F1 score for CNN, PN, MS-MLN, MoProNet, SSMN, and SSAWPN in 3-shot and 5-shot tasks of the SL1, with the best results presented in bold. As shown in Table 10, in both the 3-shot and 5-shot tasks, the F1 score of each method almost improves with the increase of the N_{TR} value. Furthermore, the F1 scores of each method are almost better in the 5-shot task compared to the 3-shot task. This indicates that increasing the quantity of fault data for each health state in the training set can provide more abundant fault information for the diagnostic framework, enhancing its diagnostic accuracy. It is worth noting that the F1 scores of SSAWPN are higher than those of the comparison approaches. The average F1 score of the SSAWPN outperforms CNN, PN, MS-MLN, MoProNet, and SSMN by 22.73 %, 1.97 %, 4.46 %, 3.45 %, and 3.21 %, respectively. In general, the few-shot learning-based methods (PN, MS-MLN, MoProNet, SSMN, and SSAWPN) significantly outperform the traditional deep learning model (CNN) in F1 score, which indicates that the traditional deep learning method struggles to achieve satisfactory results in few-shot fault diagnosis tasks. In contrast, the few-shot learning approaches are more effective in data-scarce environments, leading to better experimental results.

To better illustrate the classification performance of each approach, the confusion matrix results for the 5-shot $N_{TR} = 20$ task of the SL1 are presented in Fig. 12. From Fig. 12(a), although CNN has a good diagnosis accuracy for the three health states of NM, CF-1, and EO-1, it is difficult to identify other fault types and even completely misclassifies RO-1 as other fault types. This suggests that in data-scarce scenarios, CNN struggles to accurately and consistently recognize different fault types due to its limited learning capacity. Figs. 12(b)-(f) show that PN, MS-MLN, MoProNet, SSMN, and SSAWPN have relatively stable recognition accuracy for each fault type without complete misclassification. The results indicate that the scenario-based strategy adopted in few-shot learning enables effective feature extraction for each fault type, leading to superior performance on new diagnostic tasks. Obviously, the classification accuracy of SSAWPN outperforms the other five comparison methods. The confusion matrix results further highlight the superiority of SSAWPN.

The t-SNE visualization visually shows the feature extraction capabilities of each method in the 5-shot $N_{TR} = 20$ task of the SL1, as illustrated in Fig. 13. Fig. 13(a) shows that the classification boundaries of each health state in CNN are quite fuzzy, with significant overlap between category samples. This indicates that CNN struggles to learn the feature distribution of each category due to limited data. Fig. 13(b) illustrates that compared with CNN, the two health states of EO-1 and FWE-1 are correctly classified in PN, and the degree of aliasing between the remaining categories is also reduced. From Fig. 13(c) to (f), it can be seen that SSMN obtains the clear feature classification boundaries of the CF-1, NM, and FWE-1. Additionally, the features of four health states in MS-MLN, MoProNet, and SSAWPN are correctly clustered with clear classification boundaries. Overall, the meta-learning strategy facilitates more effective modeling of sample feature distributions, enhances the diagnostic framework's capability to distinguish each fault category, and demonstrates clear advantages in scenarios with limited fault samples. Among them, SSAWPN exhibits a superior aggregation effect for category features compared to the other methods, effectively enhancing the distinction between different categories.

4.3.2. *Case two: few-shot fault diagnosis for AHU*

In this case, comparative experiments are conducted using the AHU dataset to evaluate the adaptability and robustness of the proposed

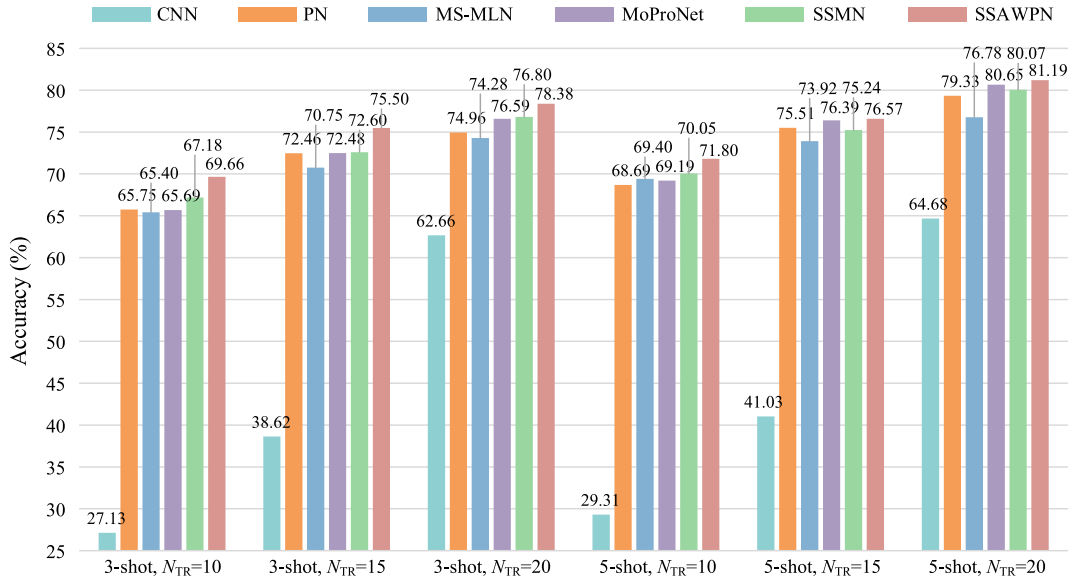

Fig. 14. The accuracy of each method on dataset two (summer).

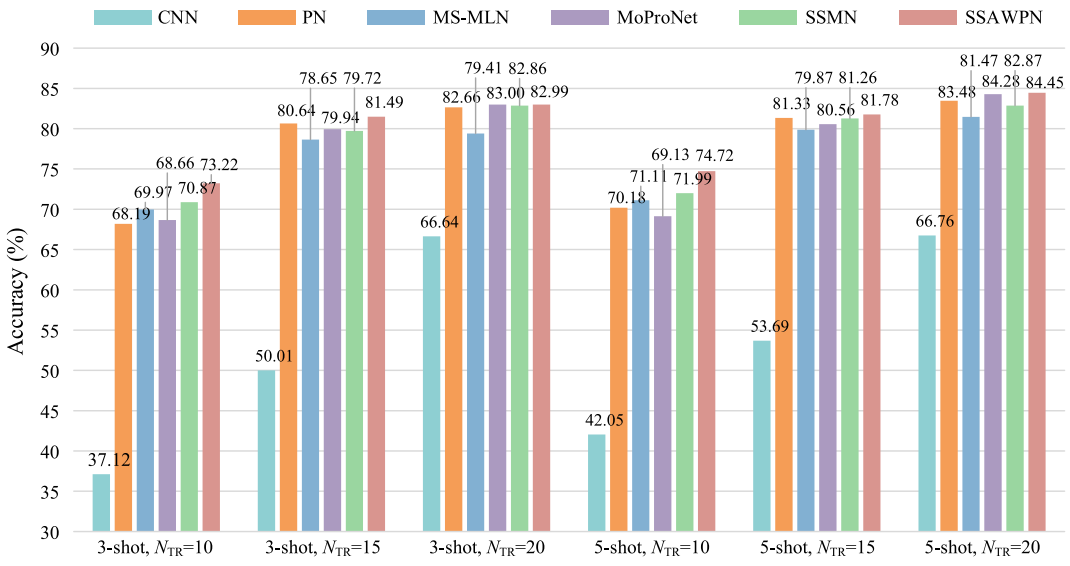

Fig. 15. The accuracy of each method on dataset two (winter).

method under different operating conditions. A detailed description of the dataset is provided in Section 4.1.2. The experiments are performed on two representative seasonal subsets (summer and winter) under 3-shot and 5-shot tasks to assess the framework's diagnostic capability in few-shot classification scenarios. During the experiments, the value of N_{TR} is set to 10, 15, and 20, respectively. The classification accuracy results under each task are presented in Figs. 14 and 15.

Fig. 14 shows that the highest and lowest average accuracy of CNN in 3-shot and 5-shot tasks are 64.68 % and 27.13 %, which are 16.51 % and 42.53 % lower than the best accuracy (81.19 %) and the lowest accuracy (69.66 %) of SSAWPN, respectively. Although the performance of CNN improves significantly with an increasing number of training samples, it still fails to achieve satisfactory results under limited fault sample conditions. PN achieves the highest and lowest average accuracy of 79.33 % and 65.75 % in the 3-shot and 5-shot tasks, respectively. Compared to CNN, PN demonstrates a stronger ability to extract fault features under few-shot conditions, leading to better diagnostic performance. The highest and lowest average accuracy of MoProNet in 3-shot and 5-shot tasks are 80.65 % and 65.69 %, respectively. Except for the 3-shot N_{TR} = 10 task, the average accuracy of MoProNet is better than that of PN in other diagnostic tasks. Furthermore, MoProNet demonstrates overall better performance than CNN and MS-MLN. This shows that MoProNet can extract rich fault features of AHUs by utilizing convolution kernels of different sizes. SSMN enhances performance by utilizing

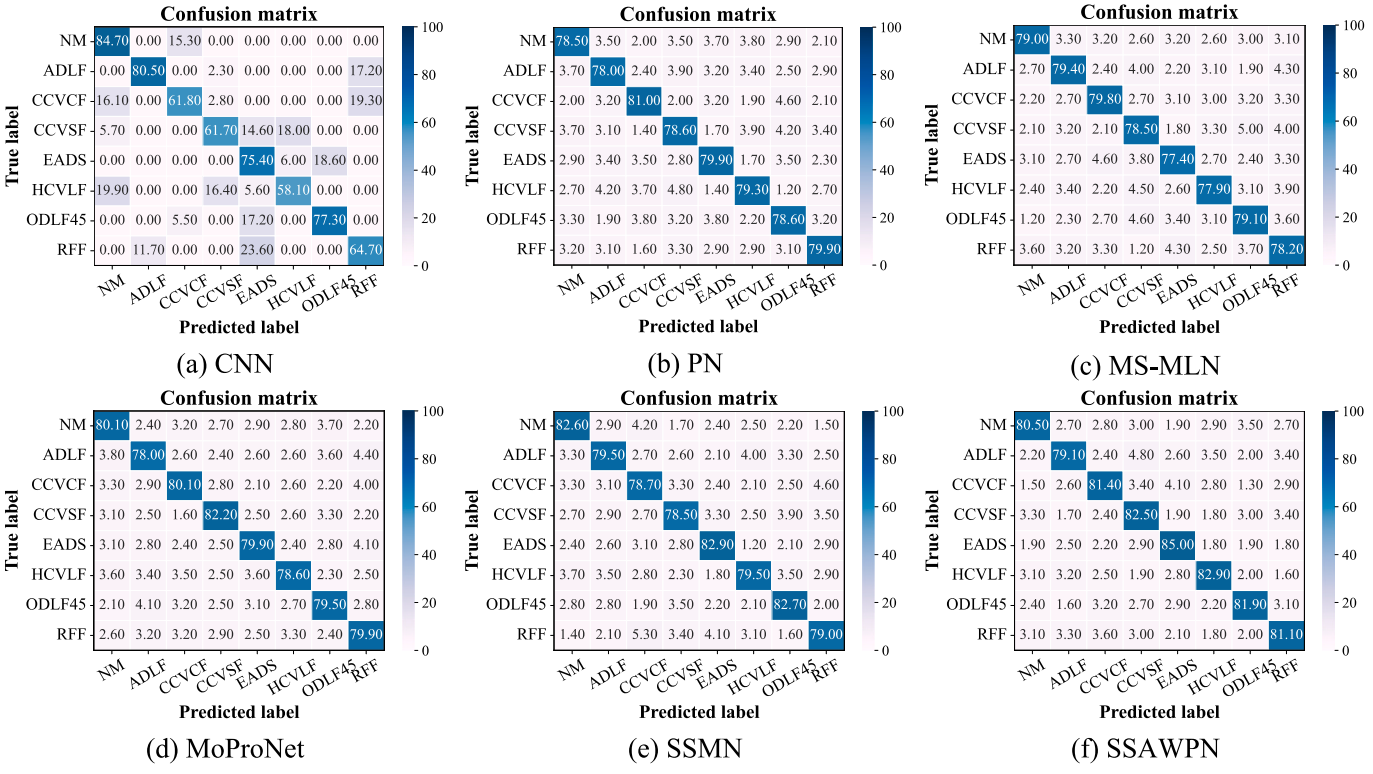

Fig. 16. Confusion matrix results on dataset two (summer) for the 5-shot task with N_{TR} = 20.

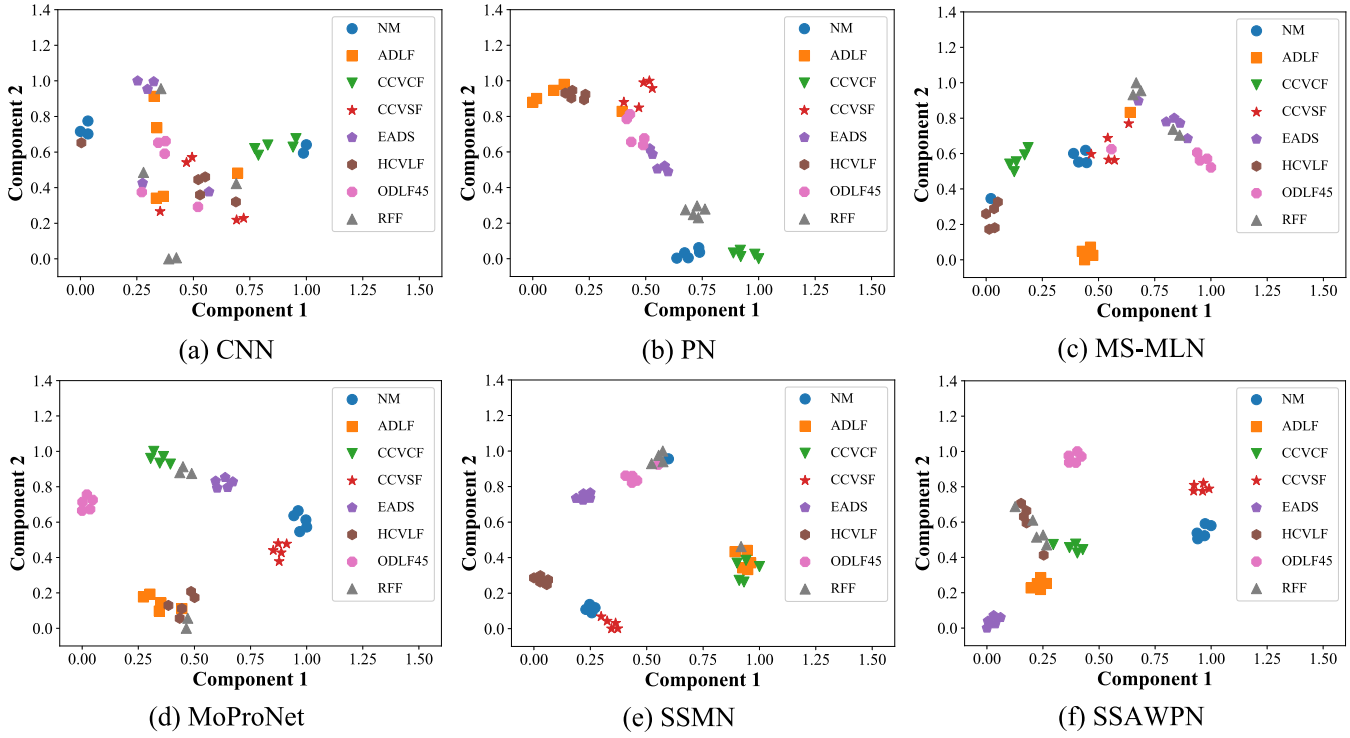

Fig. 17. t-SNE results on dataset two (summer) for the 5-shot task with $N_{TR} = 20$.

unlabeled fault samples to optimize the prototype representations. Its highest accuracy (80.07 %) and lowest accuracy (67.18 %) in 3-shot and 5-shot tasks are 1.12 % and 2.48 % lower than the highest accuracy (81.19 %) and lowest accuracy (69.66 %) of SSAWPN, respectively. On average, SSAWPN achieves an accuracy of 75.52 %, outperforming CNN (43.91 %), PN (72.78 %), MS-MLN (71.75 %), MoProNet (73.50 %), and SSMN (73.66 %) by margins of 31.61 %, 2.73 %, 3.76 %, 2.02 %, and 1.86 %, respectively. The results from the winter dataset, as illustrated in Fig. 15, reveal a similar performance trend. CNN continues to lag behind the other approaches. Specifically, SSAWPN achieved an average accuracy of 79.78 %, outperforming SSMN (78.26 %), PN (77.75 %), MoProNet (77.60 %), MS-MLN (76.75 %), and CNN (52.71 %) by 1.51 %, 2.03 %, 2.18 %, 3.03 %, and 27.07 %, respectively. Overall, results from both the summer and winter datasets confirm the superior performance and adaptability of SSAWPN in fault diagnosis tasks for AHUs with scarce fault data.

As further illustrated in Figs. 14 and 15, most methods achieve higher accuracy on the winter dataset, indicating that fault diagnosis is more challenging in the summer dataset. This performance discrepancy can be attributed to the characteristics and severity levels of the faults in each dataset. As indicated in Table 4, the winter dataset contains higher severity faults, which are generally easier to detect and classify, thereby contributing to improved diagnostic accuracy. The increased difficulty of the summer dataset underscores its value in assessing the diagnostic ability of methods under real-world scenarios. To facilitate a more comprehensive evaluation, the F1 scores, confusion matrices, and t-SNE visualizations of various models on the AHU summer dataset are further compared, as shown in Table 11, Fig. 16, and Fig. 17, respectively.

Table 11 presents the F1 scores of each method in the summer dataset under the 3-shot and 5-shot tasks. The results indicate that, in the 3-shot and 5-shot tasks with $N_{TR} = 20$, MoProNet and SSMN exhibit comparable performance, with minimal differences in F1 scores. CNN consistently lags behind the other comparison methods in all the diagnosis tasks. In contrast, MoProNet and SSAWPN with the multi-scale learning strategy obtain better F1 scores. Except for the 5-shot $N_{TR} = 15$ task, where the F1 score of SSAWPN is slightly lower than that of MoProNet, SSAWPN significantly outperforms the other five comparison methods in other diagnostic tasks. On average, SSAWPN achieves an F1 score of 67.22 %, outperforming CNN (43.71 %), PN (64.96 %), MS-MLN (64.00 %), MoProNet (65.65 %), and SSMN (65.87 %) by 23.51 %, 2.26 %, 3.22 %, 1.57 %, and 1.35 %, respectively. These results clearly demonstrate that SSAWPN delivers the most effective fault diagnosis performance in AHU and obtains satisfactory results.

The confusion matrix and t-SNE feature visualization methods provide a visual representation of the fault identification and feature extraction effects of each method in the summer dataset under the 5-shot $N_{TR} = 20$ task, as shown in Figs. 16 and 17, respectively. As shown in Fig. 16(a), CNN has good diagnosis accuracy for the health states of NM, ADLF, EADS, and ODLF45, but it is difficult to effectively identify other fault types, leading to significant misclassifications. Fig. 16(b) to (f) show that PN, MS-MLN, MoProNet, SSMN, and SSAWPN achieve better diagnosis accuracy for each health state of the AHU than CNN, with no significant misclassifications. Among them, SSAWPN demonstrates the best performance. This indicates that the fault diagnosis approaches based on few-shot learning can effectively learn the fault information of each health state under limited fault sample conditions, exhibiting strong robustness. As illustrated in Fig. 17, CNN exhibits a limited ability to accurately capture the feature distribution of each category, with significant feature aliasing observed across different fault types. Although PN, MS-MLN, MoProNet, and SSMN demonstrate improved discriminability for most fault categories, the phenomenon of feature aliasing still exists. Compared with PN, MS-MLN and MoProNet design multi-scale structures to extract more informative features, resulting in better feature clustering and separation. SSMN enhances prototype quality by incorporating information from unlabeled samples during training, thus achieving better feature representation. Notably, SSAWPN effectively clusters most of the healthy states with clear classification boundaries. This indicates that the multi-scale feature extraction strategy and the semi-supervised prototype update strategy can enhance the feature learning capability and classification accuracy of the diagnostic framework. The visualization results further demonstrate the advantages of SSAWPN in the AHU diagnosis task with limited fault samples.

Table 12
Test time of each method on the chiller and AHU datasets for the $N_{TR} = 20$ task.

Methods	3-shot (s)						5-shot (s)						Average (Ranking)
	SL1	SL2	SL3	SL4	Summer	Winter	SL1	SL2	SL3	SL4	Summer	Winter	
CNN	1.26	1.11	1.25	1.26	1.36	1.28	1.17	1.23	1.32	1.24	1.71	1.79	1.33 (1)
PN	0.26	0.24	0.26	0.27	0.31	0.26	0.36	0.37	0.36	0.32	0.83	0.38	0.35 (6)
MS-MLN	0.43	0.41	0.45	0.43	0.66	0.72	0.48	0.48	0.49	0.49	1.08	0.84	0.58 (4)
MoProNet	0.27	0.28	0.26	0.27	0.59	0.34	0.57	0.73	0.67	0.51	0.69	0.53	0.48 (5)
SSMN	0.55	0.51	0.51	0.50	0.67	0.78	0.62	0.58	0.63	0.60	1.37	1.17	0.71 (3)
SSAWPN	0.88	0.84	0.78	0.79	0.84	0.94	1.14	1.30	1.25	0.89	1.08	1.04	0.98 (2)

To comprehensively evaluate the inference efficiency of various methods across different datasets, the average testing time of each method when performing tasks with $N_{TR} = 20$ on all datasets of both the chiller system and the AHU is computed. As presented in Table 12, PN consistently achieves the best inference performance across nearly all datasets, with an average testing time of 0.35 s, significantly outperforming all other compared methods. In contrast, CNN exhibits the highest average test time at 1.33 s. Considering its relatively low testing accuracy across multiple datasets, CNN demonstrates clear limitations in scenarios with limited fault data. The average test times of MS-MLN and MoPhoNet are 0.58 s and 0.48 s, respectively. The results suggest that while multi-scale feature extraction networks can enhance diagnostic capability, they also introduce additional computational overhead. Similarly, SSMN demonstrates increased test time due to the integration of unlabeled samples for prototype optimization. SSAWPN achieves an average test time of 0.98 s, which is higher than those of PN, MS-MLN, MoPhoNet, and SSMN, but still lower than that of CNN. This reflects that although the feature extraction process based on MSAFN and the prototype optimization mechanism employed by SAWPS in SSAWPN substantially improve fault diagnosis performance, they also increase the test time. Although SSAWPN does not have the lowest test time, its superior diagnostic performance renders the relatively higher test time acceptable in practical fault diagnosis scenarios.

5. Conclusion and future work

To address the challenge of operational data scarcity in newly constructed data center HVAC systems, this study proposes a semi-supervised adaptive weighted prototypical network with attentive feature fusion. Systematic comparative and ablation experiments are conducted on the ASHRAE 1043-RP chiller dataset and the ASHRAE 1312-RP air-handling unit (AHU) dataset. These datasets comprehensively account for the range of faults that may arise during real-world operation of chillers and AHUs, with operating conditions that closely mirror field practice. Moreover, as widely recognized benchmarks in this domain, both datasets have been extensively used to support numerous state-of-art studies. The proposed method achieves satisfactory diagnostic accuracy using the above two datasets with minimal data required.

To effectively reduce reliance on both labeled and unlabeled fault samples, the proposed framework integrates the multi-scale feature extraction strategy, semi-supervised learning, and few-shot learning. Specifically, a multi-scale attentive feature fusion network is designed to effectively learn different scale features of each fault type, enhancing the fault diagnosis performance of the diagnostic framework. In addition, a semi-supervised adaptive weighted prototype optimization strategy is designed based on few-shot learning to improve the quality of prototype generation. The proposed method integrates the information of limited unlabeled fault samples into the update process of the prototype, optimizes the prototypes, and minimizes the gap between the prototypes and class centers. Ablation experiments are conducted to evaluate the effectiveness of the parameters and structure of SSAWPN. The comparison experiment results demonstrate that SSAWPN achieves competitive diagnosis results in 3-shot and 5-shot tasks, with superior fault diagnosis accuracy, robustness, and generalization performance compared to the recently published baseline methods. This research provides a practical and efficient diagnostic framework for HVAC fault diagnosis in data centers under data-scarce conditions. The main conclusions are as follows:

(1) Few-shot learning-based fault diagnosis methods exhibit superior performance compared to conventional deep learning approaches in data-scarce scenarios. Episodic training strategy significantly enhances the model's capability to distinguish different fault categories, leading to more stable and reliable diagnostic accuracy.
(2) Within the few-shot learning framework, high-performance feature extractors play a critical role in providing rich and discriminative feature representations for the prototype network. Moreover, the performance of the prototypical network directly influences diagnostic outcomes. Therefore, the development of efficient feature extraction networks and prototype learning mechanisms is key to enhancing the diagnostic capability of few-shot fault diagnosis models.
(3) The fault diagnosis framework that integrates semi-supervised learning with few-shot learning significantly reduces reliance on large-scale labeled and unlabeled datasets, while enhancing its adaptability in scenarios with limited fault data.

Although SSAWPN achieves satisfactory diagnostic results of HVAC systems with minimal data scenarios, its computational complexity is not yet optimized. In addition, clean labeled fault samples are used in this study, while noisy labels will bring adverse effects to the fault diagnosis task of the data center HVAC systems. Therefore, the following two research directions will be pursued in future work. First, the structure design of MSAFN will be further lightweighted to reduce the reasoning time required for the diagnostic framework. Second, in the fault diagnosis task with minimal training data, a confidence-based sample filtering method will be developed to mitigate the impact of unreliable operating data. In addition, we will also work towards the direction applying the proposed method to real-world building management system for more convinced soundness and robustness verifications.

CRediT authorship contribution statement

Ke Yan: Data curation, Conceptualization. **Changfu He:** Funding acquisition, Formal analysis. **Chuan Wang:** Methodology, Investigation. **Yuan Gao:** Project administration, Methodology, Investigation. **Yang Du:** Validation, Supervision, Software. **Afshin Afshari:** Writing – review & editing, Writing – original draft, Visualization.

Declaration of competing interest

The authors declare that they have no known competing financial interests or personal relationships that could have appeared to influence the work reported in this paper.

Acknowledgements

This work is supported by National Natural Science Foundation of China Excellent Young Overseas Talents Programme under Grant No. Z202304392531 and The Science and Technology Innovation Program (Overseas Expert Program) of Hunan Province under Grant No. 2024RC9006.

Data availability

Partial testing data is available in the open-source code at: https://github.com/changfuhe2020/SSAWPN

References

[1] Tervo S, Syri S, Hiltunen P. Reducing district heating carbon dioxide emissions with data center waste heat – region perspective. Renew Sust Energ Rev 2025;208:114992.
[2] Data Centers, Data transmission networks, tracking report. Available online: https://www.iea.org/reports/datacentres-and-data-transmission-networks [accessed on 15 January 2021].
[3] Zhan L, Li G, Xu C, Ren H, Sun Y. Experience knowledge decomposition – data generation: enhanced multi-step short-term cooling load predictions in data centres with data shortage issues. Energy 2025;328:136476.
[4] Public Data on Data Centre Energy Use. 2025. Available online: https://www.iea-4e.org/wp-content/uploads/2024/06/DC2b_Data_Registration_Schemes_v1.pdf [accessed in November 2024].
[5] Chan YH, Wang YF, Chan KC, Lin K, Ho TC, Tso CY, et al. Energy saving potential of passive radiative cool coating in high-rise data center with neighboring infrastructure. Energy 2024;312:133540.
[6] American Society of Heating. Refrigerating and air-conditioning engineers (ASHRAE). ANSI/ASHRAE standard 90.4–2022: Energy standard for data Centers. Atlanta, GA: ASHRAE; 2022.
[7] Centers Data, Facilities Telecommunications. Chapter 20. ASHRAE HVAC Applications, https://www.ashrae.org/technical-resources/ashrae-handbook/2023-ashrae-handbook-hvac-applications; 2023.
[8] Lawrence Berkeley National Laboratory document: https://datacenters.lbl.gov/resources/thermal-guidelines-and-temperature. 2025.
[9] Kargar S, Moran JL. Combining direct and indirect free cooling for data centers via transformation into a building-scale heat exchanger. Appl Energy 2025;392:125973.
[10] Wu S, Zheng W, Wang Z, Chen G, Yang P, Yue S, et al. AlphaDataCenterCooling: a virtual testbed for evaluating operational strategies in data center cooling plants. Appl Energy 2025;380:125100.
[11] Jones N. How to stop data centres from gobbling up the world's electricity. Nature 2018;561:163–6.
[12] Qin H, Meng T, Chen K, Li Z. A comparative study of DQN and D3QN for HVAC system optimization control. Energy 2024;307:132740.
[13] Zou M, Huang W, Jin J, Hu B, Liu Z. Deep spatio-temporal feature fusion learning for multi-step building cooling load forecasting. Energ Buildings 2024;322:114735.
[14] Ni H, Liu C, Li Y, Chong W, Chou J. Enhancing HVAC energy efficiency modeling in semiconductor manufacturing facilities using tree-structured parzen estimator-optimized deep learning. Build Environ 2025;271:112589.
[15] Giraldo-Pérez J, Bruse J, Odriozola J, Mejía-Gutiérrez R. Balancing indoor air quality and ventilation efforts via deep reinforcement learning: An agent-based approach applied to an office building. Energ Buildings 2025;335:115501.
[16] Lei L, Li Z. A novel dynamic predictive control model for variable air volume air conditioning systems using deep learning. J Build Eng 2024;95:110314.
[17] Jung D, Byun H, Choi I, Lee J. Analysis of the impact of supply air temperature on outdoor unit power consumption in EHP-AHU systems and development of a DNN-based predictive model. Energ Buildings 2025;341:115812.
[18] Tang L, Xie H, Wang Y, Xu Z. Deeply flexible commercial building HVAC system control: a physics-aware deep learning-embedded MPC approach. Appl Energy 2025;388:125631.
[19] Zhang L, Chen Z. Large language model-based interpretable machine learning control in building energy systems. Energ Buildings 2024;313:114278.
[20] Nisa E, Kuan Y, Lin C. Leveraging multi-zone building data with machine learning-based models and genetic algorithms to optimize air handling units. J Build Eng 2024;96:110411.
[21] Sulaiman M, Mustaffa Z, Saealal M, Saari M, Ahmad A. Utilizing the Kolmogorov-Arnold networks for chiller energy consumption prediction in commercial building. J Build Eng 2024;96:110475.
[22] Lu R, Li X, Chen R, Lei A, Ma X. An alternative reinforcement learning (ARL) control strategy for data center air-cooled HVAC systems. Energy 2024;308:132977.
[23] Guo F, Ham S, Kim D, Moon HJ. Deep reinforcement learning control for co-optimizing energy consumption, thermal comfort, and indoor air quality in an office building. Appl Energy 2025;377:124467.
[24] Díaz F, Montes J, Villamor J, Fernández S. Enhancing and optimization in exisiting HVAC equipment using tools of industry 4.0. J Build Eng 2025;102:111924.
[25] Ni H, Liu C, Paul F, Chong W, Chou J. Enhancing supply chain resilience and efficiency of HVAC systems in semiconductor manufacturing facilities using graph-based large multimodal models. Appl Energy 2025;398:126420.
[26] Yao L, Huang L, Teo J. HVAC control based on reinforcement learning and fuzzy reasoning: optimizing HVAC supply air temperature, flow rate, and velocity. J Build Eng 2025;103:112143.
[27] Ni H, Chong WO, Chou J. Optimizing HVAC systems for semiconductor fabrication: a data-intensive framework for energy efficiency and sustainability. J Build Eng 2024;89:109397.
[28] Ding X, Cerpa A, Du W. Multi-zone HVAC control with model-based deep reinforcement learning. IEEE T Autom Sci Eng 2025;22:4408–26.
[29] Li Y, Liu C, Ni H, Paul F, Chong WO, Chou J. Generative artificial intelligence-based framework for bridging lifecycle gaps in semiconductor HVAC systems. J Build Eng 2025;105:112349.
[30] Lu C, Ma X, Yan K. Chiller fault diagnosis based on improved variational autoencoder and co-training framework: a case study of insufficient samples. J Build Eng 2024;88:109137.
[31] Deshmukh S, Samouhos S, Glicksman L, Norford L. Fault detection in commercial building VAV AHU: a case study of an academic building. Energ Buildings 2019;201:163–73.
[32] Tran D, Chen Y, Chau M, Ning B. A robust online fault detection and diagnosis strategy of centrifugal chiller systems for building energy efficiency. Energ Buildings 2015;108:441–53.
[33] Lin G, House J, Chen Y, Granderson J, Zhang W. Active multi-mode data analysis to improve fault diagnosis in AHUs. Energ Buildings 2025;337:115621.
[34] Han H, Zhang Z, Cui X, Meng Q. Ensemble learning with member optimization for fault diagnosis of a building energy system. Energ Buildings 2020;226:110351.
[35] Xia Y, Ding Q, Li Z, Jiang A. Fault detection for centrifugal chillers using a kernel entropy component analysis (KECA) method. Build Simul-China 2021;14:53–61.
[36] Li P, Liu Z, Anduv B, Zhu X, Jin X, Du Z. Diagnosis for multiple faults of chiller using ELM-KNN model enhanced by multi-label learning and specific feature combinations. Build Environ 2022;214:108904.
[37] Simmini F, Rampazzo M, Peterle F, Susto G, Beghi A. A self-tuning KPCA-based approach to fault detection in chiller systems. IEEE T Contr Syst T 2022;30:1359–74.
[38] Li G, Chen L, Liu J, Fang X. Comparative study on deep transfer learning strategies for cross-system and cross-operation-condition building energy systems fault diagnosis. Energy 2023;263:125943.
[39] Liu J, Zhang Q, Li X, Li G, Liu Z, Xie Y, et al. Transfer learning-based strategies for fault diagnosis in building energy systems. Energ Buildings 2021;250:111256.
[40] Zhu X, Chen K, Anduv B, Jin X, Du Z. Transfer learning based methodology for migration and application of fault detection and diagnosis between building chillers for improving energy efficiency. Build Environ 2021;200:107957.
[41] Jiang K, Gao X, Gao H, Han H, Qi Y. VIT-GADG: a generative domain-generalized framework for chillers fault diagnosis under unseen working conditions. IEEE T Instrum Meas 2023;72:1–13.
[42] Miyata S, Kuwahara Y, Tsunemoto S, Tanaka K, Akashi Y. Improving training efficiency for scalable automated fault detection and diagnosis in chilled water plants by transfer learning. Energ Buildings 2023;285:112877.
[43] Shen C, Zhang H, Meng S, Li C. Augmented data driven self-attention deep learning method for imbalanced fault diagnosis of the HVAC chiller. Eng Appl Artif Intell 2023;117:105540.
[44] Zhang H, Yang W, Yi W, Lim JB, An Z, Li C. Imbalanced data based fault diagnosis of the chiller via integrating a new resampling technique with an improved ensemble extreme learning machine. J Build Eng 2023;70:106338.
[45] Fan Y, Cui X, Han H, Lu H. Chiller fault diagnosis with field sensors using the technology of imbalanced data. Appl Therm Eng 2019;159:113933.
[46] Wang H, Bi J, Hua M, Yan K, Afshari A. Semi-supervised CWGAN-GP modeling for AHU AFDD with high-quality synthetic data filtering mechanism. Build Environ 2025;267:112265.
[47] Yang W, Zhang H, Lim JB, Zhang Y, Meng H. A new chiller fault diagnosis method under the imbalanced data environment via combining an improved generative adversarial network with an enhanced deep extreme learning machine. Eng Appl Artif Intell 2024;137:109218.
[48] Peng Y, Wang Y, Shao Y. A novel bearing imbalance fault-diagnosis method based on a Wasserstein conditional generative adversarial network. Measurement 2022;192:110924.
[49] Yan K, Huang J, Shen W, Ji Z. Unsupervised learning for fault detection and diagnosis of air handling units. Energ Buildings 2020;210:109689.
[50] Du Z, Chen K, Chen S, He J, Zhu X, Jin X. Deep learning GAN-based data generation and fault diagnosis in the data center HVAC system. Energ Buildings 2023;289:113072.
[51] Yan K, Chong A, Mo Y. Generative adversarial network for fault detection diagnosis of chillers. Build Environ 2020;172:106698.
[52] Zhang J, Li Z, Chen H, Cheng H, Xing L, Wang Y, et al. Integrated generative networks embedded with ensemble classifiers for fault detection and diagnosis under small and imbalanced data of building air condition system. Energ Buildings 2022;268:112207.
[53] Yan K, Lu C, Ma X, Ji Z, Huang J. Intelligent fault diagnosis for air handing units based on improved generative adversarial network and deep reinforcement learning. Expert Syst Appl 2024;240:122545.
[54] Li B, Cheng F, Cai H, Zhang X, Cai W. A semi-supervised approach to fault detection and diagnosis for building HVAC systems based on the modified generative adversarial network. Energ Buildings 2021;246:111044.

[55] Beghi A, Brignoli R, Cecchinato L, Menegazzo G, Rampazzo M, Simmini F. Data-driven fault detection and diagnosis for HVAC water chillers. Control Eng Pract 2016;53:79–91.
[56] Yan K, Zhong C, Ji Z, Huang J. Semi-supervised learning for early detection and diagnosis of various air handling unit faults. Energ Buildings 2018;181:75–83.
[57] Li B, Cheng F, Zhang X, Cui C, Cai W. A novel semi-supervised data-driven method for chiller fault diagnosis with unlabeled data. Appl Energy 2021;285:116459.
[58] Fan C, Liu Y, Liu X, Sun Y, Wang J. A study on semi-supervised learning in enhancing performance of AHU unseen fault detection with limited labeled data. Sustain Cities Soc 2021;70:102874.
[59] Deng Q, Chen Z, Tang P, Li X, Yang C, Yang X. A novel semi-supervised fault diagnosis method for chillers based on neighbor-optimized graph convolutional network. Energ Buildings 2023;301:113703.
[60] Fan C, Lin Y, Piscitelli MS, Chiosa R, Wang H, Capozzoli A, et al. Leveraging graph convolutional networks for semi-supervised fault diagnosis of HVAC systems in data-scarce contexts. Build Simul-CHINA 2023;16:1499–517.
[61] Ma G, Ding H. Semi-supervised random Forest methodology for fault diagnosis in air-handling units. Buildings 2023;13:14.
[62] Ren Z, Han H, Cui X, Lu H, Luo M. Novel data-pulling-based strategy for chiller fault diagnosis in data-scarce scenarios. Energy 2023;279:128019.
[63] Albayati M, Faraj J, Thompson A, Patil P, Gorthala R, Rajasekaran S. Semi-supervised machine learning for fault detection and diagnosis of a rooftop unit. Big Data Mining and Analytics 2023;6:170–84.
[64] Fan C, Wu Q, Zhao Y, Mo L. Integrating active learning and semi-supervised learning for improved data-driven HVAC fault diagnosis performance. APPL ENERG 2024;356:122356.
[65] Han H, Gao X, Han H, Gao H, Qi Y, Jiang K. Non-parametric semi-supervised chiller fault diagnosis via variational compressor under severe few labeled samples. Eng Appl Artif Intell 2025;146:110233.
[66] Ren M, Triantafillou E, Ravi S, Snell J, Swersky K, Tenenbaum J. Meta-learning for semi-supervised few-shot classification. In: 6th int conf learn represent ICLR 2018 - conf track proc; 2018. p. 1–15.
[67] Feng Y, Chen J, Zhang T, He S, Xu E, Zhou Z. Semi-supervised meta-learning networks with squeeze-and-excitation attention for few-shot fault diagnosis. ISA T 2022;120:383–401.
[68] Lao Z, He D, Jin Z, Liu C, Shang H, He Y. Few-shot fault diagnosis of turnout switch machine based on semi-supervised weighted prototypical network. Knowl-Based Syst 2023;274:110634.
[69] Snell J, Swersky K, Zemel R. Prototypical networks for few-shot learning. In: Proceedings of the 31st International Conference on Advance Neural Information Process System; 2017. p. 4078–90.
[70] Hu J, Shen L, Sun G. Squeeze-and-excitation networks. IEEE/CVF Conference on Computer Vision and Pattern Recognition 2018;2018:7132–41.
[71] Yan K, Zhou X. Chiller faults detection and diagnosis with sensor network and adaptive 1D CNN. Digit Commun Netw 2022;8:531–9.
[72] Wang Y, Liu S. A multi scale meta-learning network for cross domain fault diagnosis with limited samples. J Intell Manuf 2025;36:2841–61.
[73] Chen X, Yang R, Xue Y, Yang C, Song B, Zhong M. A novel momentum prototypical neural network to cross-domain fault diagnosis for rotating machinery subject to cold-start. Neurocomputing 2023;555:126656.
[74] He C, He D, Wei Z, Xu K, Chen Y, Shan S. A train bearing imbalanced fault diagnosis method based on extended CCR and multi-scale feature fusion network. Nonlinear Dynam 2024;112:13147–73.
[75] Van der Maaten L, Hinton G. Visualizing High-Dimensional Data Using t-SNE. J Mach Learn Res 2008;9:2579–605.
[76] Comstock M, Braun J, Bernhard R. Experimental data from fault detection and diagnostic studies on a centrifugal chiller. Purdue University; 1999.
[77] Wen J, Li S. Tools for evaluating fault detection and diagnostic methods for air handling units. ASHRAE RP-1312 Final Report. Atlanta: American Society of Heating, Refrigerating and Air Conditioning Engineers Inc.; 2011.
[78] Yan K, Chen X, Zhou X, Yan Z, Ma J. Physical model informed fault detection and diagnosis of air handling units based on transformer generative adversarial network. IEEE T IND Inform 2023;19:2192–9.
[79] Yun W, Hong W, Seo H. A data-driven fault detection and diagnosis scheme for air handling units in building HVAC systems considering undefined states. J Build Eng 2021;35:102111.